TITLE:

Signaling and functional bias at the human complement C5a receptors

INTRODUCTION:

G protein-coupled receptors (GPCRs), also referred to as seven transmembrane receptors (7TMRs), constitute a large family of cell surface proteins in the human genome with direct involvement in all major physiological processes[1,2]. The overall transducer coupling framework of these receptors is highly conserved across the family where agonist activation results in the coupling of heterotrimeric G proteins followed by phosphorylation, primarily by GPCR kinases (GRKs), at multiple sites, and subsequent binding of β-arrestin 1 and 2 (βarr1 and 2; also known as arrestin2 and 3) [3,4]. While natural agonists typically induce both G protein and βarr coupling to these receptors, it is possible to design ligands that promote preferential coupling to one of these transducers leading to biased signaling[5,6]. The selective targeting of one of the signaling pathways paves the way for designing novel drugs with reduced side effects.

The signaling bias is manifested at multiple levels, for example, in terms of G-protein subtype-selectivity, engagement of GRK sub-types, or βarr isoform preference. However, a key question remains unanswered: Are there any examples of naturally existing biased 7TMRs that selectively recruit one of the two well-known transducers, i.e., G-proteins and βarrs? In humans, a class of chemokine receptors known as Atypical Chemokine Receptors (ACKRs) and a complement peptide receptor(C5aR2) represent a classic example of intrinsically biased receptors, also known as Non-canonical GPCRs[5,7–10]. These receptors bind to the same endogenous ligands as canonical GPCRs; however, unlike canonical GPCRs, they do not exhibit any functional G-protein coupling, although they can interact with βarrs upon agonist stimulation. Some examples of Canonical/Non-canonical receptor pairs include human complement C5a receptor pair, C5aR1 and C5aR2[11], the chemokine receptor2 CCR2, and human decoy D6 receptor[9] (D6R/ACKR2) and the CXC chemokine receptor 4, CXCR4 and the CXC chemokine receptor 7, CXCR7(ACKR3)[5]. Although there are scattered hints in the literature suggesting these 7TMRs exhibit agonist-induced βarr recruitment, they are poorly characterized in terms of comprehensive G-protein coupling profile, GRK-dependence, βarr conformational signatures, and downstream signaling.

Our work focuses on two distinct complement C5a receptors, C5aR1 and C5aR2, as a model system to gain insights into the various aspects such as ligand-binding, transducer coupling, and downstream signaling of C5a receptors. Both of these receptors share a common seven transmembrane architecture, and they are activated by a common natural agonist, C5a (Figure 1).

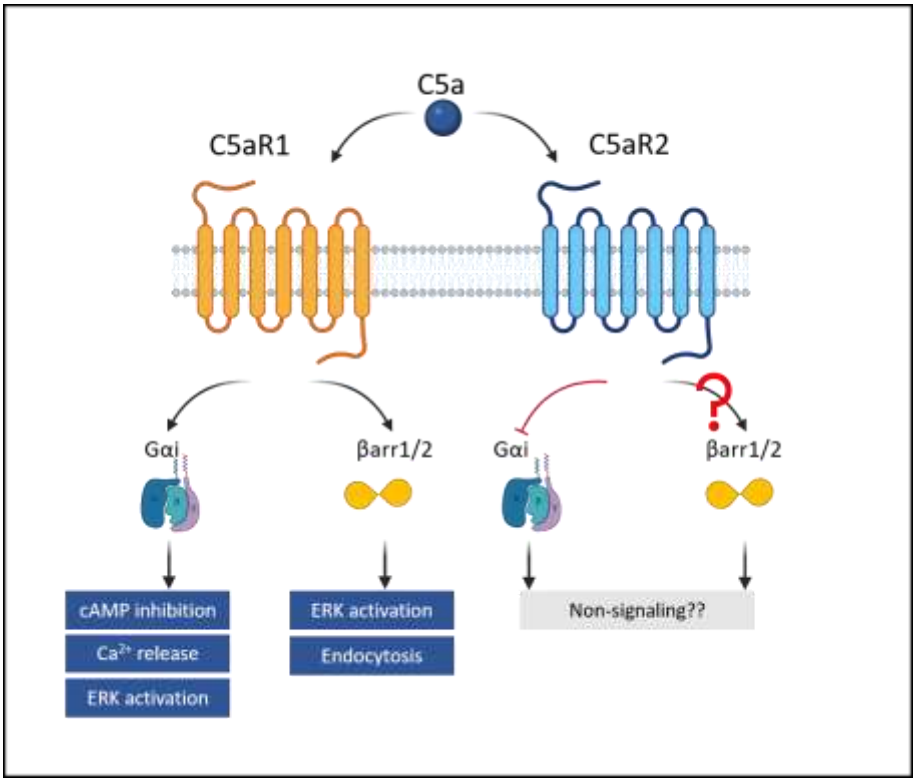

Figure 1. Schematic representation of canonical and non-canonical C5a receptors and their signaling capabilities.

The structure of human C5a consists of four different helices and connecting loops, which are stabilized by the formation of three disulfide bonds[12]. As per the two-site binding model, C5a binds to C5aR1 through two distinct subsites: the first site of interaction involves the core of C5a and the N terminus of the receptor, whereas the second site of interaction includes the C terminus of C5a and the extracellular region of the TM helices of C5aR1 [13] (Figure 2).

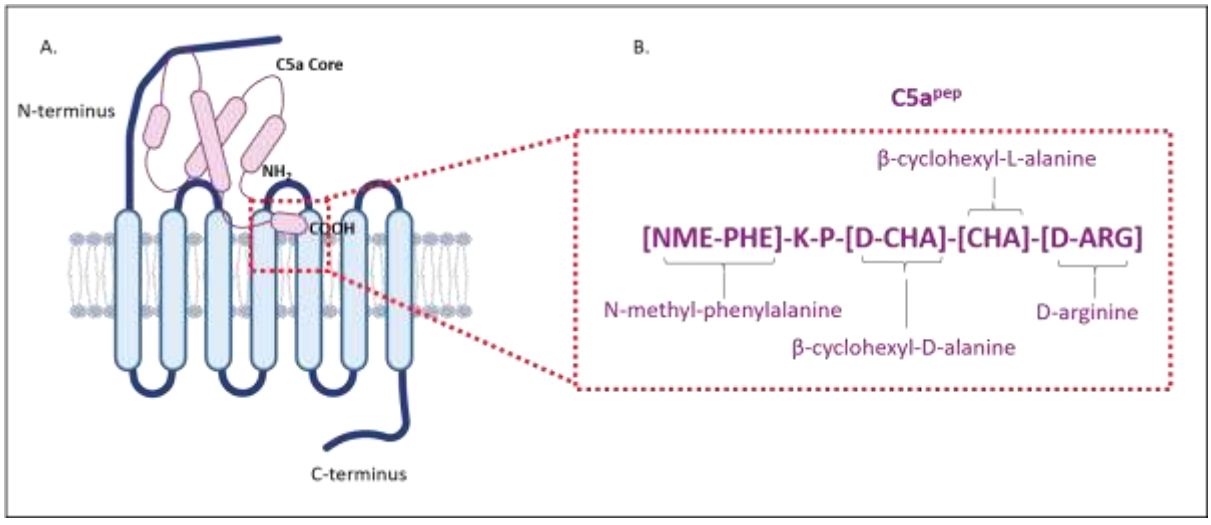

Figure 2 The schematic representation of a synthetic C-terminal peptide derived from C5a. A. C5a binds to C5aR1 at distinct sites involving the N-terminus and extrahelical part of the transmembrane

region of the receptor. **B.** $C5a^{pep}$ is a modified hexapeptide derived from the carboxyl terminus of C5a *(Adapted from Pandey S. et al. JBC, 2019)* [14]

It has been proposed that the first set of interactions is responsible for the high-affinity binding of C5a to C5aR1, whereas the second set of interactions plays a critical role in driving receptor activation. Peptides derived from the carboxy terminus of C5a can bind to C5aR1, and they can also trigger functional responses, but their binding affinities are much less than C5a [15,16]. However, the possibility of whether such peptides may induce differential transducer coupling and initiate a functionally selective response has not been explored.

Using a combination of biochemical, functional and cellular approaches, we have discovered that a carboxyl-terminal fragment of C5a serves as a functionally-biased ligand at C5aR1 by inducing distinct transducer-coupling, trafficking and signaling patterns. More importantly, we have also discovered that C5aR2 couples to, and signals through βarrs, but not G-proteins, upon C5a-stimulation, and therefore, it is an intrinsically βarr-biased receptor. Finally, We have reconstituted C5aR2-βarr complexes *in-vitro* for structural analysis using cryogenic electron microscopy (cryo-EM), which sets the stage to visualize the complex at high resolution going forward. Taken together,our findings reveal previously unknown functional-bias in the C5a-C5aR system, and provide a framework to decipher novel structural and functional insights into biased signaling through 7TMR scaffold.

OBJECTIVES:

- To explore the phenomena of ligand bias for complement C5a receptors.
- To understand the different transducer coupling patterns for C5aR1 and C5aR2.
- To elucidate βarr recruitment and GRK isoform preference for C5aR1 and C5aR2.
- To dissect the unexplored signaling pathways for non-canonical seven transmembrane receptors.

MATERIALS AND METHODS:

Cloning and construct design

The human C5aR1 and C5aR2 coding regions were cloned in pcDNA3.1 vector with the N-terminal HA signal sequence followed by a FLAG tag, and the coding regions of bovine βarr1 and βarr2 were cloned in the pCMV vector.

Cell Culture

Different cell lines were cultured as per the recommended conditions. Chinese hamster ovary (CHO) cells stably expressing the human C5aR1 (CHO-C5aR1) were cultured in Ham's F-12 growth medium

containing 10% fetal bovine serum (FBS), 100 units/ml penicillin, 100 µg/ml streptomycin, and 400 µg/ml geneticin (G418, Invivogen). Human embryonic kidney-293 (HEK-293) cells were grown in DMEM containing 10 % FBS, 100 IU/ml penicillin, and 100 µg/ml streptomycin under 37°C, 5 % CO_2 condition. All cell lines were maintained in 10 cm plates T175 flasks or (37 °C, 5 %CO2) and passaged at 80–90% confluency using 0.05 % Trypsin-EDTA and D-PBS. Cell morphology was monitored continually to keep the consistency of cell function in check, and cell lines were not used beyond passage 20-25.

For the generation of Human monocyte-derived macrophages (HMDM), human buffy coat blood was procured through the Australian Red Cross Blood Service from anonymous healthy donors. Human CD14+ monocytes were extracted from the blood using Lymphoprep density centrifugation (STEMCELL) followed by CD14+ MACS magnetic bead separation. The isolated monocytes were differentiated in IMDM containing FBS(10 %), penicillin(100 U/ml), streptomycin (100 µg/ml), and recombinant human macrophage colony-stimulating factor (15 ng/ml) (M-CSF) on 10-mm square dishes (Sterilin) for 7 days. The cells were washed with DPBS to get rid of the non-adherent cells. Afterward, the adhered and differentiated HMDMs were harvested by scraping gently.

Human polymorphonuclear cells (PMNs) were collected from whole venous blood (20 ml) taken from healthy volunteers with informed consent. The blood samples were collected using venepuncture into BD K2EDTA Vacutainer®collection tubes and processed within 5 hours of collection. For neutrophil isolation, the anticoagulated blood was first layered over a Lymphoprep density gradient and subjected to centrifugation (800 X g for 30 min, 22 °C). After centrifugation, the residual erythrocytes were removed using hypotonic lysis. The separated PMNs were first counted and then resuspended in a migration buffer (1X HBSS buffer containing calcium, magnesium,0.5 % BSA, and 20 mM HEPES).

ERK1/2 phosphorylation in HEK293 cells

Agonist-induced ERK1/2 activation was measured primarily using a previously described Western blotting–based protocol [17]. C5aR1 or C5aR2-expressing stable cell lines were seeded at a density of 1 million cells per well of a 6-well tissue culture plate. The cells were subjected to serum-starvation for 12 h followed by stimulation with either 1 µM of C5a or 10 µM of $C5a^{pep}$ at selected time points. After the stimulation, the incomplete growth medium was removed, and the cells were lysed in 100 µl of 2XSDS dye/well by gentle scraping. The cell lysates were boiled at 95 °C for 15 min and cleared by centrifugation at 15,000 rpm for 10 min. 10 µl of the cellular lysate was loaded and separated on SDS-PAGE followed by immunoblotting. The PVDF membranes were blocked in 5% BSA (in 1XTBST) for 1 hour and incubated overnight with rabbit phospho-ERK1/2 primary antibody (1:5000). The

membranes were washed thrice for 10 min each with 1XTBST and incubated with anti-rabbit HRP-coupled antibody (1:10,000) for 1 hour. The membranes were rewashed with TBST three times to remove unbound secondary antibody and developed with Promega ECL chemiluminescent solution on chemidoc (Bio-Rad). The membranes were stripped with low pH stripping buffer and then reprobed for total ERK using rabbit total ERK primary antibody (1:5000). To investigate the effect of PTX treatment on ERK1/2 phosphorylation, cells stably expressing C5aR1 were seeded in a 6-well plate and 8 hours of seeding pretreated with 100 ng/ml PTX for 12–16 hours followed by serum starvation. After completion of serum starvation, the cells were stimulated with either C5a or $C5a^{pep}$ for the specified time points. The cells were lysed in 2X loading dye, and samples were prepared as described previously.

Agonist induced receptor internalization

HEK-293 cells at 50-60% confluency were transfected with 3.5 µg of FLAG-tagged C5aR1 DNA using 21 µg of PEI (DNA: PEI ratio 1:3). 24 hours after transfection, 0.15 million cells were seeded in each well of 24-well plate already coated with 0.01 % poly-D-lysine. After 18-24 hours of seeding, the cells were serum-starved for approximately 6 hours followed by stimulation with either 1 µM of C5a and 10 µM $C5a^{pep}$ for indicated time points. Post-agonist-stimulation, the cells were washed once with ice-cold 1XTBS. The cells were then fixed using 4 % (w/v) paraformaldehyde (PFA) on ice for 20 min and washed with TBS to remove excess PFA. Blocking was done in the presence of 1 % BSA prepared in 1XTBS for 1.5 hours. Afterward, the cells were incubated with HRP-conjugated anti-FLAG M2 antibody (1:2000) prepared in 1 % BSA (in 1XTBS) for 1.5 h at room temperature. Afterward, the cells were rewashed with 1 %BSA (in 1XTBS) to remove traces of antibodies. Receptor surface expression was measured by incubating cells with 200 µl of 3,3',5,5'-tetramethylbenzidine (TMB-ELISA) per well till blue color appeared, and the reaction was quenched (before saturation) by transferring 100 µl of colored TMB to a 96-well plate already containing 100 µl of 1 M H_2SO_4. Absorbance at 450 nm was recorded in a multiplate reader (Victor X4). For normalization with total cell density, the cell density was measured using Janus green B. Briefly, TMB was removed, and the cells were washed twice with 1XTBS followed by staining of cells with 0.2 % Janus green B (w/v) for 15 min. De-staining was performed by extensively washing the cells with 1 ml of distilled water. The stain was eluted using 800 µl of 0.5 N HCl, and 200 µl of the eluted solution was transferred to a 96-well plate. The absorbance was read at 595 nm, and data were normalized by calculating the ratio of A450 to A595 values.

GloSensor assay for cAMP measurement

To measure the inhibition of cAMP response using GloSensor assay, HEK-293 cells were co-transfected with either C5aR1 or C5a-V_2R (3.5 µg) and 22F (3.5µg) plasmids. After 16-18 hours of transfection, the cells were trypsinized with the trypsin-EDTA solution and harvested by centrifugation (1500 rpm, 10 min). The supernatant was aspirated, and cells were finally resuspended in luciferin sodium solution (0.5 mg/ml) prepared in drug buffer (1X HBSS and 20 mM HEPES, pH 7.4). Afterward, the cells were counted in a hemocytometer and then seeded at a density of 0.4 million/well in a white flat-bottom 96-well plate. The cells were kept in the CO_2 incubator at 37°C for 1.5 h, followed by additional incubation of 30min at room temperature in the dark. Basal readings were recorded on luminescence mode of multiplate reader (Victor X4), and cycles were adjusted until basal luminescence values were stable. After recording the basal reading, the cells were treated with 1µM forskolin, and luminescence was read on the plate reader until luminescence values were stabilized after reaching maxima. The cells were then treated with a specified concentration range of either C5a or $C5a^{pep}$, and values were recorded for 30 cycles (1 hour). The basal correction was performed by subtracting basal readings from luminescence readings recorded after ligand stimulation. The data normalization was performed with respect to a minimal ligand dose and plotted in GraphPad Prism 8.0.

Crosslinking and coimmunoprecipitation of βarrs with C5aR1

To analyze the interaction of C5aR1 with βarrs in response to C5a and $C5a^{pep}$, we transfected 50-60% confluent HEK-293 cells with either C5aR1 or C5a-V_2R along with βarr1/βarr2 plasmids by PEI transfection method. After 48 hours, the cells expressing receptor and βarrs were subjected to serum starvation for 6 hours and stimulated with saturating doses of C5a (100 nM)/ $C5a^{pep}$(1 µM), harvested, and proceeded for the cross-linking experiment. Briefly, the cells were lysed by Dounce homogenization in 20 mM HEPES, pH 7.4, 100 mM NaCl, 1X PhosSTOP cocktail, 2 mM benzamidine hydrochloride, and 1 mM PMSF. After homogenization, cross-linking was performed by the addition of 1 mM DSP crosslinker from a fresh 100 mM stock (dissolved in DMSO). The lysate was tumbled at room temperature for 40 min, and the cross-linking reaction was stopped by adding 1 M Tris, pH 8.5. The cell lysates were solubilized in the presence of 1% (v/v) MNG for 1 hour by gentle tumbling at room temperature. The cellular lysates were cleared by centrifugation (15,000 rpm, 15 min, 4°C). Cleared supernatant containing cross-linked protein complex was then transferred to a separate tube already containing pre-equilibrated M1 antibody conjugated-agarose beads supplemented with 2 mM $CaCl_2$. The reaction mix was tumbled for 2 hours at 4°C to allow bead binding. The beads were washed with low salt buffer (20 mM HEPES, pH 7.4, 150 mM NaCl, 2 mM $CaCl_2$, and 0.01% MNG) and high salt buffer (20 mM HEPES, pH 7.4, 350 mM NaCl, 2 mM $CaCl_2$, and 0.01% MNG), respectively to remove non-specifically bound proteins. The protein complex captured on FLAG beads was eluted in FLAG-

elution buffer (20 mM HEPES, 150 mM NaCl, 2 mM EDTA, 250 µg/ml FLAG peptide, and 0.01% MNG). βarr after coimmunoprecipitation was detected by running the eluted protein samples on SDS-PAGE followed by immunoblotting using rabbit anti-βarr mAb (1:5000). The membranes were stripped with low pH stripping buffer and reprobed for the receptor (C5aR1 or C5a-V_2R) with HRP-coupled anti-FLAG M2 antibody (1:5000). The blots were developed using a chemiluminescent solution from Promega on Chemidoc (Bio-Rad) and quantified using ImageLab software (Bio-Rad).

Chemotaxis assay in human PMN

Human PMN migration in response to C5a and $C5a^{pep}$ was assessed using 6.5-mm Transwell polycarbonate membrane inserts with 3.0-µm to create a modified Boyden chamber (31). First, freshly isolated hPMNs were seeded onto membrane inserts at a cell density of 500,000 per well for 20 min (37 °C, 5% CO2) in an HBSS-containing migration buffer (as mentioned previously. To initiate cell migration, either C5a or $C5a^{pep}$ (prepared in migration buffer) were added to the receiver wells in duplicates. After 60 min of agonist-induced migration (37 °C, 5% CO2), the membrane inserts were gently washed once with PBS, and after that, the residual cells on the upper part of the membrane were removed carefully using a cotton swab. For detaching the migrated cells, 500µl of Accumax solution (Invitrogen) was added to each well of the receiver wells and incubated for 10 min at room temperature. Afterward, the cells were counted using a Bio-Rad TC20TM automated cell counter. For PTX treatment, freshly isolated hPMNs were incubated with 3 µg/ml PTX or vehicle control only and seeded onto inserts with a cell density of 500,000 per well (37 °C, 5% CO2) in migration buffer. After incubation with PTX for 4 hours, cell migration was assessed as mentioned above.

Measurement of interleukin-6 release using ELISA

The immunomodulatory effect of C5a and $C5a^{pep}$ ligands on LPS-induced IL-6 release was monitored in HMDMs (34). The macrophages were seeded in 96-well tissue culture plates at a density of 100,000 per well for 24 hours before ligand addition. The ligands were diluted in serum-free IMDM supplemented with 0.1% BSA. After preparing the ligands, the cells were co-treated with LPS and respective ligands for 24 hours at 37 °C, 5% CO_2. The supernatant media was collected and stored at -20°C till use. The levels of IL-6 in the supernatant were quantified using appropriate human ELISA kits (BD OptEIA) as per the manufacturer's protocol.

NanoBiT G protein dissociation assay

NanoBiT-G-protein dissociation assay was performed to measure agonist-induced G protein activation [18], where the dissociation of heterotrimeric G protein into Gα and Gβγ subunit was monitored by a

NanoBiT system (Promega). Briefly, a NanoBiT-G-protein consisting of a large fragment (LgBiT)-containing Gα subunit and a small fragment (SmBiT)-tagged $G\gamma_2$ subunit with a C68S mutation, along with the untagged $G\beta_1$ subunit, was expressed in HEK-293A cells with a test GPCR construct, and the ligand-induced change in luminescent signal was measured. HEK-293A cells were seeded in a 6-well culture plate at a concentration of 2 x 10^5 cells/ml (2 ml per dish hereafter) in DMEM supplemented with 10% FBS, glutamine, penicillin, and streptomycin, one day before transfection. The transfection mix was prepared by combining 5 µl of polyethylenimine solution (1 mg/ml) and a plasmid mixture consisting of 100 ng LgBiT-Gα, 500 ng $G\beta_1$, 500 ng SmBiT-$G\gamma_2$ (C68S), and an indicated volume (below) of either C5aR1 or C5aR2 in 200 µl of Opti-MEM. The receptor constructs used for the G protein dissociation assay harbored an N-terminal HA-derived signal sequence and FLAG-epitope tag followed by a flexible linker (MKTIIALSYIFCLVFADYKDDDDKGGSGGGGSGGSSSGGG; ssHA-FLAG-GPCR). To measure dissociation of the other G-protein subtypes, LgBiT-$G\alpha_s$ subunit (G_s), LgBiT-$G\alpha_q$ subunit (G_q), and LgBiT-$G\alpha_{13}$ subunit (G_{13}) were transfected in the cells instead of the LgBiT-$G\alpha_{i1}$ subunit plasmid. To enhance NanoBiT-G-protein expression for G_s, G_q, and G_{13}, 100 ng plasmid of RIC8B (isoform 2; for G_s) or RIC8A (isoform 2; for G_q and G_{13}) was additionally co-transfected. To match the expression of C5aR1 and C5aR2 to a similar level, 40 ng of C5aR1 (total DNA was made up to 200ng with an empty vector) and 200 ng of C5aR2 plasmids were used. The next day, the transfected cells were harvested with 0.5 mM EDTA-containing Dulbecco's PBS, centrifuged, and resuspended in 2 ml of assay buffer containing 1X HBSS, 0.01% BSA, and 5 mM HEPES (pH 7.4). The cells suspended in the assay buffer were seeded in a white 96-well plate at a volume of 80 µl per well, followed by the addition of 20 µl of 50 µM coelenterazine diluted in the assay buffer. After 2 hours of incubation, the plate was measured for baseline luminescence (SpectraMax L, Molecular Devices) and 20 µl of C5a(working stock of 6X concentration), serially diluted in the assay buffer, was manually added. After ligand addition, the luminescence was immediately recorded for the second measurement as a kinetics mode, and the counts recorded from 3 min to 5 min after ligand addition were averaged and normalized to the initial counts. The fold-change signals were further normalized to the vehicle-treated signal and were plotted as a G-protein dissociation response. The G-protein dissociation signals were plotted using a four-parameter sigmoidal concentration-response curve in the Prism 8 software (GraphPad Prism).

Reconstitution of C5aR2-βarr1-Fab30 complex and negative stain electron microscopy

To reconstitute a complex of C5aR2 with βarr1, we overexpressed Flag-tagged WT C5aR2, along with $GRK2^{CAAX}$ and βarr1 in *Sf9* cells using the baculovirus expression system. 66 hours after infection, the cells were treated with 100nM C5a for 1 hour at 27°C, and the complex using was subsequently

stabilized with Fab30. Afterward, the complex purification was performed by FLAG-affinity chromatography using anti-Flag M1 antibody agarose and size exclusion chromatography. Before negative staining, the protein complex was diluted to 0.02 mg/ml in a buffer containing 20 mM HEPES, pH7.4, and 150 mM NaCl. Negative staining of the protein complex was conducted according to the published protocols [19]. Briefly, 3.5 µl of the complex was added onto glow discharged formvar/carbon-coated 300 mesh copper grids, and excess solution was blotted off after adsorption of the sample using a filter paper for 60 seconds. Negative staining was performed for nearly 45 seconds using a freshly prepared uranyl formate stain (0.75 % (w/v). After negative staining, the samples were imaged using a LaB6 120kV transmission electron microscope (FEI Tecnai G2 12 Twin TEM) mounted with a Gatan CCD camera (4k x 4k) at 30,000x magnifications. Nearly 10,000 particles were selected manually from 118 micrographs using e2boxer.py from the EMAN2.31 software suite [20]. Afterward, 2D image classification was performed with ISAC2 [21] from the SPHIRE suite [22] using the box files generated from EMAN2.31.

NanoBiT βarr recruitment assay

To measure agonist-induced βarr recruitment in GRK-KO cells, we performed a NanoBiT-βarr recruitment assay. Briefly, the parental HEK-293A, GRK2/3-KO, GRK5/6-KO, and GRK2/3/5/6-KO cells [23] were seeded and transfected as per the protocol described in the "NanoBiT-G-protein dissociation assay" section. For the βarr recruitment assay, we transfected the respective cells with 100 ng (hereafter per well in a 6-well plate) of an N-terminally LgBiT-fused βarr1/2 plasmid, 80 ng C5aR1 (420 ng of an empty vector) or 500 ng C5aR2 and a C-terminal SmBiT (ssHA-FLAG-GPCR-SmBiT). The NanoBiT luminescence was measured from the transfected cells as described above. Luminescence counts from 10 min to 15 min after C5a addition were used for the calculation.

Ib30 NanoBiT recruitment assay

To measure the reactivity of Intrabody 30 (Ib30) for βarr1 in the context of C5aR1 and C5aR2 NanoBiT assay was performed [24]. βarr1 and Ib30 were fused at the N-terminus to SmBiT and LgBiT, respectively, with a flexible linker containing and inserted in the pCAGGS plasmid. The surface expression of C5aR1 (0.25 µg) and C5aR2 (3 µg) was matched to a similar level was by DNA titration, and transfections were performed accordingly. Briefly, the HEK-293 cells were transfected with either C5aR1 or C5aR2, LgBiT-Ib30 (5 µg), and SmBiT βarr1 (2 µg) at 3 million cell density using PEI as transfection agent (DNA: PEI ratio of 1:3). After 16-18 hours of transfection, cells were harvested by centrifugation in PBS solution supplemented with 0.5 mM EDTA. Afterward, the cells were resuspended in 3 ml of HBSS containing assay buffer (1XHBSS buffer, 0.01% BSA and 5 mM HEPES, pH 7.4) containing coelenterazine at 10 µM

final concentration. The cells were then seeded at a density of 70,000 cells per 100 µl per well in a white, clear-bottom 96 well plate. The plate was incubated at 37°C for 1.5 hours in the CO_2 incubator, followed by an additional incubation of 30 min at room temperature. Basal luminescence readings were recorded on the multi-plate reader (Victor X4) using luminescence protocol. Afterward, the cells were treated with varying concentrations of C5a (6x stock, 20 µl per well) ranging from 0.1 pM to 1 µM diluted in drug buffer (HBSS buffer with 5 mM HEPES, pH 7.4). The luminescence readings were recorded for 60 min after ligand addition. Basal correction was performed by averaging the initial counts of 4-10 cycles. Fold increase was measured with respect to vehicle control values, and analysis was performed using a nonlinear regression four-parameter sigmoidal dose response curve in GraphPad Prism 8.0 software.

FlAsH BRET experiments

To assess the conformational changes in βarr2 upon interaction with C5aR1 and C5aR2, we measured agonist-induced change in fluorescence using FlAsH BRET assay. Briefly, HEK-293SL cells were seeded at a density of 1.5×10^5 cells per well in a 6-well plate one day before transfection and then transfected the next day with either C5aR1 or C5aR2 and βarr2-FlAsH constructs using the calcium phosphate co-precipitation method of transfection. 24 hours after transfection, cells were seeded at a density of 2.5×10^4 cells per well in poly-ornithine-coated white, clear-bottom 96-well plates. The next day, cells were washed and incubated with Tyrode's buffer (140 mM NaCl, 2.7 mM KCl, 1 mM $CaCl_2$, 12 mM $NaHCO_3$, 5.6 mM D-glucose, 0.5 mM $MgCl_2$, 0.37 mM NaH_2PO_4, and 25 mM HEPES, pH 7.4) for 1 hour at room temperature. FlAsH labeling was performed using a previously described protocol [25]. Briefly, 1.75 µl of FlAsH-EDT_2 reagent was mixed with 3.5 µl of 25 mM EDT solution (dissolved in DMSO) and incubated at room temperature for 10 min. 100 µl of Tyrode's buffer was added to the reaction mix and left for 5 min at room temperature. Afterward, the reaction volume was adjusted to 5 ml with Tyrode's buffer to complete the labeling solution. Prior to labeling, the cells were washed with Tyrode's buffer followed by incubation with 60 µl of labeling solution per well for 1 hour at 37°C. After labeling, the cells were first washed twice with BAL wash buffer and then with Tyrode's buffer. Next, 90 µl of Tyrode's buffer was added to the cells in each well followed by incubation for 1 hour at 37°C. Afterward, the cells were treated with 1 µM C5a for 10 min, with six consecutive BRET measurements recorded every minute after 5 min ligand addition. Coelenterazine H, at a final concentration of 2 µM, was added 3 min before BRET measurements and readings were taken in triplicates for each condition. BRET signals were recorded using a Victor X (PerkinElmer) plate reader with a filter setting (center wavelength) of 460/25 nm (donor) and 535/25 nm (acceptor). BRET ratios were calculated by taking a ratio of the intensity of light emitted by the acceptor over the intensity of light emitted by the donor.

The net BRET ratio was calculated by subtracting the unlabeled BRET signal (background) from the FlAsH-EDT_2-labeled BRET signal. The net change in the BRET signal (ΔnetBRET) was obtained by dividing the net BRET ratio after stimulation by the vehicle net BRET ratio.

Phospho antibody array

A phospho-antibody array from Full Moon Biosystems consisting of over 1300 phosphosite specific antibodies against proteins from multiple signaling pathways was used to discover potential signaling pathways downstream of C5aR2. The samples were prepared as per the manufacturer's protocol and sent to Full Moon Biosystems for further analysis. Briefly, HEK-293 cells stable cell lines expressing the receptor were stimulated with saturating concentration of C5a (100nM) for 10 min and then harvested using 1 ml of ice-cold 1X PBS supplemented with 0.01% Phosphatase inhibitor (PhosSTOP). Cell pellets corresponding to 10 plates of a 10 cm culture dish were pooled together and harvested at 5,000 rpm for 5 min at 4˚C. After discarding the supernatant, the cell pellets were rewashed with ice-cold 1X PBS to remove any traces of media. Unstimulated HEK-293 cells stably expressing the receptor were used as a control. Samples were prepared separately under similar conditions for three independent sets and sent to Full Moon Biosystems for phosphor-antibody array and analysis. The antibody array was performed using the manufacturer's kit (Cat. no. KAS02). Briefly, cells were lysed using a lysis buffer, and the lysate was cleared by centrifugation. Before biotin labeling, the buffer was exchanged to ensure proper protein biotinylation. The total protein was estimated using the BCA protein estimation method for both unstimulated and stimulated conditions, and an equal amount of lysate was used for the experiment for the stimulated and unstimulated conditions. Afterward, biotinylated proteins were incubated with the immobilized antibodies coated on a glass slide. After extensive washing, the biotinylated proteins bound to respective antibodies were detected using Cy3 streptavidin. The signal for phosphoproteins was finally detected using a microarray scanner. The signal ratio was calculated after dividing the fluorescence signal for the stimulated sample by the corresponding unstimulated sample.

Ligand induced p90RSK phosphorylation in HEK293 cells

HEK-293 cells stably expressing C5aR2 were seeded in 10 cm culture dishes at a density of 5 million to measure C5a-induced p90RSK phosphorylation. After 18-24 hours of seeding, cells were serum starved in serum free growth medium for 16 hours followed by stimulation with 100 nM C5a for different time points and harvested in PBS. Afterward, the cells were lysed in 200 µL of 2XSDS reducing buffer, and cellular lysates were boiled for 30 min at 95°C followed by centrifugation at 15000 rpm for 15 min. Subsequently, 10 µL of cell lysate was loaded in each well and separated on SDS-PAGE followed by

western blotting. The blocking of PVDF membranes was done in 5% BSA (in TBST) for 1 hour followed by an overnight incubation with phosphorylation site-specific p90RSK primary antibodies (phospho-Thr^{359}, 1:500; phospho-Thr^{573}, 1:500; phospho-$SerS^{380}$, 1:500). The next day, blots were washed thrice with TBST for 10min each and incubated with anti-rabbit HRP-coupled secondary antibody for 1 hour. To remove the secondary antibody, blots were washed thrice with 1XTBST again and developed with Promega ECL solution on chemidoc (BioRad). The PVDF membranes were stripped using a stripping buffer to remove phospho-specific antibody and then re-probed for total RSK (RSK1/RSK2/RSK3) using a rabbit monoclonal primary antibody at 1:2500 dilution. The signals were normalized by dividing the phospho-site specific signal from the corresponding total RSK signal.

Human monocyte-derived macrophages

Human monocyte-derived macrophages (HMDM) were obtained and cultured as per the previously described protocol [26,27]. Briefly, human buffy coat blood was obtained from anonymous healthy donors through the Australian Red Cross Blood Service (Brisbane, Australia). Human $CD14^+$ monocytes were isolated from blood using Lymphoprep density centrifugation followed by $CD14^+$ MACS separation (described in Chapter2). The isolated monocytes were cultured in IMDM supplemented with 10% FBS, 100 U/ml penicillin, 100 µg/ml streptomycin, and 15 ng/ml recombinant human M-CSF (macrophage colony-stimulating factor) on 10 mm square dishes (Bio-strategy, Brisbane, Australia). The adherent differentiated HMDMs were collected by gentle scraping on Day 6-7.

In cell western assays in HMDMs

We performed in-cell western assays to detect the phosphorylation of p90RSK in HMDMs as per the technical guidelines from LI-COR Biosciences (Lincoln, USA). Briefly, HMDMs were seeded at a density of 80,000 cells per well in poly D-lysine-coated black-wall clear-bottom tissue culture 96-well plates for 24 hours and subjected to serum-starvation overnight. All ligands were prepared in serum-free growth media containing 0.1% BSA. Cells were first pre-treated with the C5aR1 selective antagonist PMX53 (10 µM) for 20 min (37 ℃, 5 % CO_2) followed by stimulation with recombinant human C5a (100nM) or P32 (100 µM) at room temperature for 10 min. The media was removed, and the cells were fixed using 4 % paraformaldehyde for 10 min at room temperature). After gently washing with DPBS, the cells were permeabilized using ice-cold methanol for 10 min at room temperature and then blocked using Odyssey Blocking Buffer in TBS for 1.5hour at room temperature. The cells were then incubated with the phospho-specific primary antibodies at 4℃ overnight (phospho-$p90RSK^{S380}$, 1:800; phospho-$p90RSK^{T359}$, 1:200; phospho-$p90RSK^{T573}$, 1:200). Upon further washing with DPBS containing 0.1 % Tween-20, the cells were stained with IRDye 680RD donkey anti-rabbit secondary antibody

(1:1000) and/or IRDye 800CW donkey anti-mouse IgG secondary antibody (1:1000) for 1.5 hours at room temperature. The plate was then washed with DPBS containing 0.1 % Tween-20 and blotted dry. For fluorescence quantification, the plate was read on a Tecan Spark 20M microplate reader (Ex/Em: 667 nm/ 707 nm for IRDye 680RD and 770 nm/810 nm for IRDye 800CW, respectively) (Tecan, Männedorf, Switzerland).

Enzyme linked immunosorbent assay

Blood from WT, C5aR1$^{-/-}$ and C5aR2$^{-/-}$ mice was collected in tubes containing 4 mM EDTA, and plasma was separated by centrifugation for 10 min at 2000xg at 4°C. TNFα levels in plasma were determined using a commercially available enzyme-linked immunosorbent assay kit (BD Biosciences).

RESULTS:

C5a^{pep} is a low potency agonist for Gαi activation

Although previous studies have demonstrated that C5a^{pep} has a greater binding affinity for C5aR1 compared to other peptides derived from the C terminus of C5a, its binding affinity for C5aR1 is still significantly less than C5a (∼1 nM for C5a and∼70 nM for C5a^{pep})[15]. We, therefore, first assessed the ability of C5a^{pep} to trigger Gα$_i$ activation downstream of C5aR1 using the GloSensor assay in HEK-293 cells [28]. As C5aR1 is primarily a Gα$_i$ coupled receptor, we measured agonist-induced inhibition of cAMP response as a readout for Gα$_i$ coupling (Figure 3A). The cells expressing C5aR1 were first treated with forskolin to generate cAMP, followed by incubation with a concentration range(10^{-11}M to 10^{-6}M) of C5a and C5a^{pep}. We discovered that both C5a and C5a^{pep} led to inhibition of forskolin-induced cAMP levels in a similar fashion at saturating concentrations (Figure 3B). As reflected from their binding affinities for the receptor, C5a^{pep} was ∼100-fold less potent than C5a in causing inhibition of cAMP (IC_{50} = ∼16 nM for C5a^{pep} and IC_{50} = ∼0.26 nM for C5a). Additionally, we investigated the efficacy of C5a^{pep} using the LANCE cAMP assay in a different cellular context, where C5aR1 expressing CHO cells were treated with saturating doses of C5a and C5a^{pep} [29]. We observed a similar pattern of ligand efficacy and potency that we had observed in HEK-293 cells (Figure 3C).

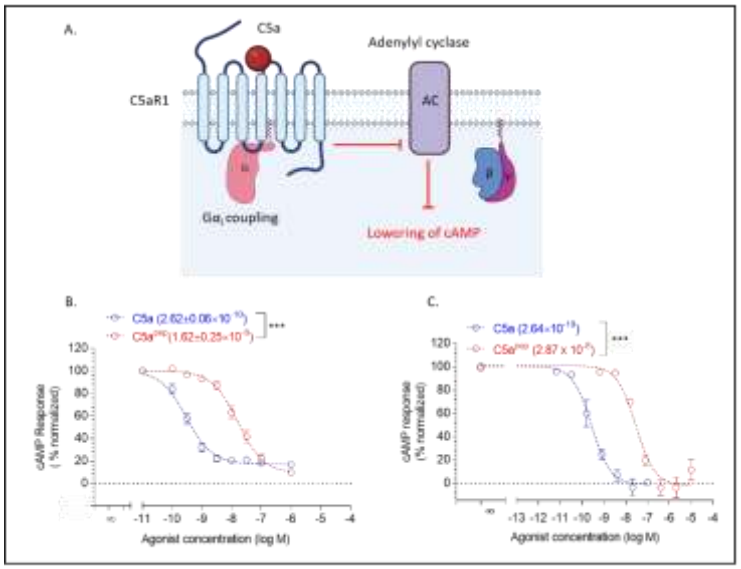

Figure 3 C5a^{pep} is a full agonist for Gαi coupling. A. Schematic representation of C5a induced cAMP inhibition. B. C5a^{pep} is a full agonist for inhibition of cAMP in GloSensor assay. HEK-293 cells co-transfected with C5aR1 and F22 plasmids were stimulated with indicated concentrations of C5a and C5a^{pep}, followed by recording the luminescence readout. C. C5a^{pep} exhibits full agonist efficacy for Gαi coupling in LANCE cAMP assay performed in CHO cells. CHO cells expressing C5aR1 were stimulated with indicated doses of C5a and C5a^{pep,} and ligand-induced change in fluorescence was recorded. The data shown in B. and C. represent the mean ± SEM of 3-5 independent experiments. The EC_{50} values of the respective ligands were analyzed using Unpaired t-test (***, p< 0.001) *(Adapted from Pandey S. et al. JBC, 2019)* [14].

C5a^{pep} behaves as a partial agonist for βarrestin recruitment

The stimulation of C5aR1 with its endogenous agonist C5a results in receptor phosphorylation. The phosphorylated receptor recruits βarrs, which play a crucial role in receptor desensitization and endocytosis, similar to other GPCRs [30,31]. Hence, we next measured the ability of C5a^{pep} to induce βarr recruitment to the receptor using a standard coimmunoprecipitation assay. As discussed in the previous chapter, the two isoforms of βarrs known as βarr1 and 2 exhibit a significant divergence in their functional outcomes despite having a high sequence and structural similarity[32]. Hence, we co-expressed either βarr1 or βarr2 with FLAG-tagged C5aR1 in HEK-293 cells to measure their interaction with the receptor in response t different ligands. As shown in Figure 4 (*A* and *B*), we observed that C5a stimulation of C5aR1 expressing cells led to robust recruitment of both isoforms of βarrs. Surprisingly, however, the level of βarr recruitment in response to C5a^{pep} was significantly less than C5a, even at saturating ligand doses. As a negative control, we treated the cells with a C5aR1 selective antagonist W54011 [33], and as expected, the W54011 treatment did not elicit any significant levels of βarr recruitment. Furthermore, to probe whether these ligands may exhibit a temporal difference in the C5aR1-βarr interaction pattern, we conducted a time-course experiment to monitor the

recruitment of βarr to C5aR1. Similar to the previous observation, we found that C5a^{pep}-induced βarr recruitment was significantly less than C5a (Figure 4, C and D). Taken together with the cAMP data shown above, our findings suggest that C5a^{pep} behaves as a full-agonist for Gα_i-coupling but as a partial agonist for βarr recruitment to C5aR1.

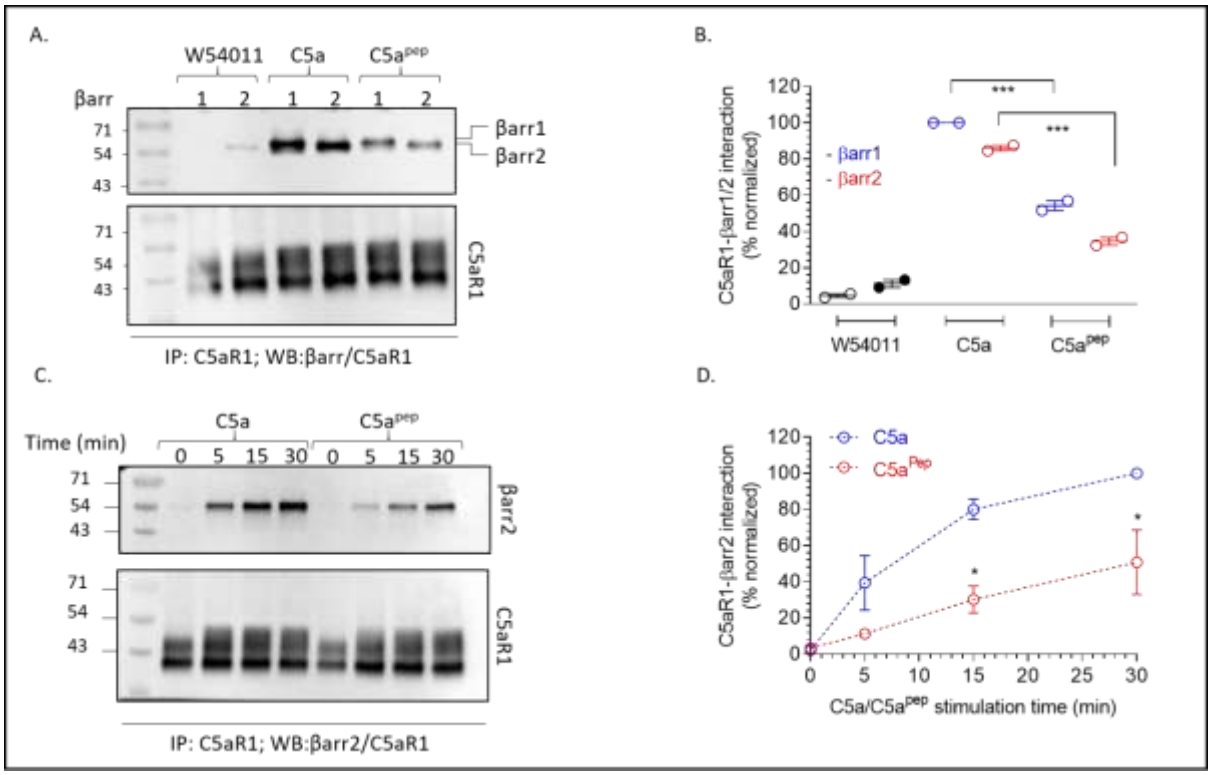

Figure 4 C5a^{pep} is a partial agonist for βarr recruitment. A. HEK-293 cells co-transfected with FLAG-tagged C5aR1 and either βarr1 or βarr2 were stimulated with saturating concentrations of W54011 (0.1 μM), C5a (1 μM) and C5a^{pep} (10 μM), followed by chemical crosslinking. βarrs were coimmunoprecipitated using agarose beads conjugated with an anti-FLAG antibody and co-eluted with FLAG peptide containing elution buffer. Eluted proteins were visualized by Western blotting using anti-βarr and anti-FLAG antibodies. **B.** Densitometric quantification of data presented in panel A (mean ± SEM of n=2). The data are normalized with respect to signal intensity of C5a-βarr1 condition treated as 100% and analyzed by Two-way ANOVA (***, p<0.001). **C.** The data represents the time-course coimmunoprecipitation of βarr2 with C5aR1 to measure their agonist-induced interaction. The experiment was performed following the same protocol mentioned in A. **D.** Densitometric quantification of data presented in panel B (mean ± SEM of n=2) normalized with respect to signal intensity of C5a at 30 min condition (treated as 100%) and analyzed by Two-way ANOVA (*, p<0.05) *(Adapted from Pandey S. et al. JBC, 2019)* [14].

C5a^{pep} is a partial agonist for endocytosis and a full agonist for ERK1/2 activation

To investigate whether C5a^{pep} binding to C5aR1 may also result in differential efficacy compared with C5a at the level of a signaling outcome, we assessed the ability of C5a^{pep} to mediate C5aR1 internalization and ERK1/2 MAP kinase phosphorylation in HEK-293 cells. In corroboration with our βarr recruitment and trafficking data, we noticed that C5a^{pep} induced lower levels of receptor

endocytosis than C5a (Figure 5 A). This observation indicates that βarrs may be critically involved in driving C5aR1 endocytosis, and therefore, weaker βarr recruitment by $C5a^{pep}$ is mirrored into lesser receptor internalization. Interestingly, however, $C5a^{pep}$ was as good as C5a in initiating the activation of ERK1/2 MAP kinase in C5aR1 expressing HEK-293 cells, at least at the time points tested in this experiment (Figure 5 B and C). Thus, the correlation of maximal levels of internalization triggered by C5a and $C5a^{pep}$ with the ERK1/2 phosphorylation reveals a signaling bias of $C5a^{pep}$ in mediating these two outcomes post-receptor activation. The full efficacy of $C5a^{pep}$ for ERK1/2 activation, similar to that observed in the cAMP assay, hints that this response may be driven by $G\alpha_i$.

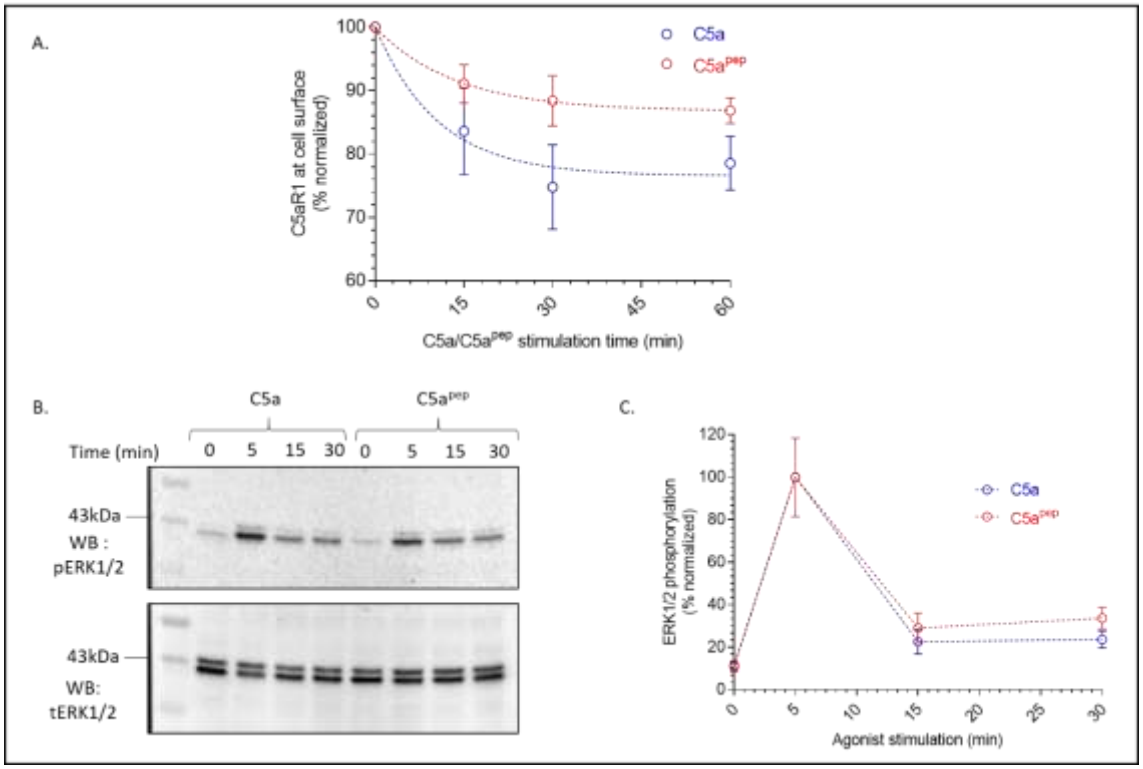

Figure 5 $C5a^{pep}$ exhibits signaling bias between receptor internalization and ERK1/2 phosphorylation. A. HEK-293 cells expressing C5aR1 were stimulated with saturating concentrations of C5a (1 µM) and $C5a^{pep}$ (10 µM) for indicated time points, and receptor surface expression was assessed by whole cell-based surface ELISA. $C5a^{pep}$ exhibits weaker efficacy than C5a in inducing C5aR1 internalization. The data represents mean ± SEM from five independent experiments. **B.** $C5a^{pep}$ behaves similar to C5a in mediating ERK1/2 phosphorylation. HEK-293 cells stably expressing C5aR1 were stimulated with the respective ligands (concentrations mentioned above) for indicated time points. ERK1/2 phosphorylation was assessed by Western-blotting with an anti-phospho ERK antibody. **C.** The data represent densitometry-based quantification (mean ± SEM of n=5 experiments) of ERK1/2 phosphorylation *(Adapted from Pandey S. et al. JBC, 2019)*[14].

$C5a^{pep}$ induces biased cellular responses in macrophages and neutrophils

Stimulating human monocyte-derived macrophages with C5a reduces the LPS-induced release of IL-6 [34], whereas the stimulation of neutrophils with C5a induces rapid chemotaxis[35]. To test whether

C5a^{pep} might exhibit a bias at the level of these cellular responses, we measured the release of IL-6 and chemotaxis in primary human monocyte-derived macrophages(HMDMs) and human polymorphonuclear neutrophils (hPMNs), respectively. We noticed that the suppression of LPS-induced IL-6 release in HMDMs was similar for both C5a and C5a^{pep} (Figure 6 A), and it was completely blocked in response to PTX pretreatment (Figure 6 *C*). Surprisingly, however, we observed that even at saturating doses, C5a^{pep} stimulation resulted in a significantly blunted response in neutrophil migration compared with C5a (Figure 6 *B*), although similar to IL-6 release, the chemotactic response was also ablated upon PTX pretreatment (Figure 6 D), suggesting that both the processes are driven by Gαi coupling to C5aR1.

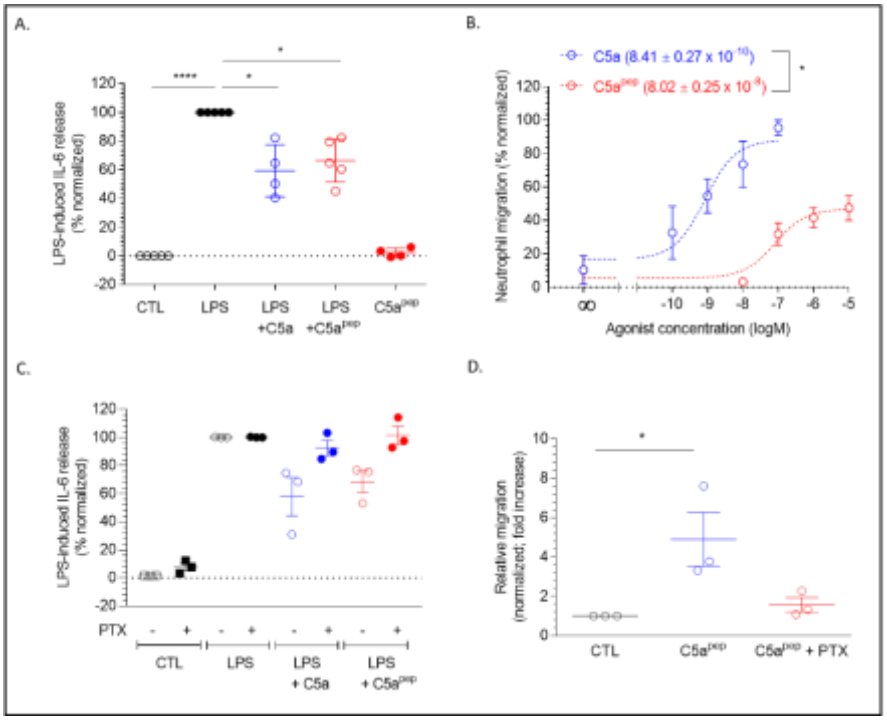

Figure 6 C5a^{pep} exhibits bias between suppression of LPS-induced IL-6 release and neutrophil mobilization. A. C5a^{pep} behaves as a full agonist for lowering LPS induced release in macrophages. HMDMs were treated with LPS (10 ng/ml) in the presence or absence of C5a or C5a^{pep}. The levels of IL-6 in the supernatant after 24 hours of stimulation were detected by ELISA and basal corrected with the values for control. The values were normalized with respect to the maximum signal for LPS (treated as 100%). The data represent mean ± SEM of experiments performed in triplicate from 4 independent donors and analyzed using Two way ANOVA (*, $p < 0.05$; ****, $p < 0.0001$). **B.** C5apep exhibits a weak agonist profile for neutrophil migration. Freshly isolated PMNs were stimulated with either C5a or C5a^{pep} at indicated concentration, and chemotaxis was assessed in the Boyden chamber for 1 h. The number of migrated cells was recorded, and normalization was done with respect to the maximal C5a-induced chemotaxis. The data were plotted as mean ± SEM of experiments conducted in triplicates from three independent donors. The EC_{50} values of C5a and C5a^{pep} were analyzed by Unpaired t-test(*, $p < 0.05$). **C.** and **D.** C5a^{pep} mediated IL-6 suppression and neutrophil migration are sensitive to PTX treatment. HMDMs and neutrophils were pretreated with PTX overnight and for 4 hours, respectively, before ligand stimulation. The IL-6 release and PMN migration were assessed after ligand stimulation,

and data were normalized as mentioned in A and B (plotted as mean ± SEM). The data analysis was performed using Two way ANOVA (*, $p < 0.05$) *(Adapted from Pandey S. et al. JBC, 2019)* [14].

C5aR2 fails to induce G protein coupling and second messenger response

Previously some of the studies have reported that agonist stimulation of C5aR2 fails to induce G-proteins to the receptor; however, the experimental data are mostly limited to a lack of cAMP or Ca^{2+} response as a readout of Gαi-activation [36]. Therefore, we first comprehensively measured the G-protein activation profile of these receptors using a NanoBiT-based G-protein dissociation assay [18] (Figure 7A). Here, we overexpressed a NanoBiT-G protein consisting of a LgBiT-Gα subunit and a SmBiT-Gγ2 subunit, untagged Gβ1 subunit along with either C5aR1 or C5aR2 construct in HEK-293 cells [18]. In these experiments, the expression of C5aR1 and C5aR2 was normalized to comparable levels as measured by flow-cytometry-based surface expression assay (Figure 7B).

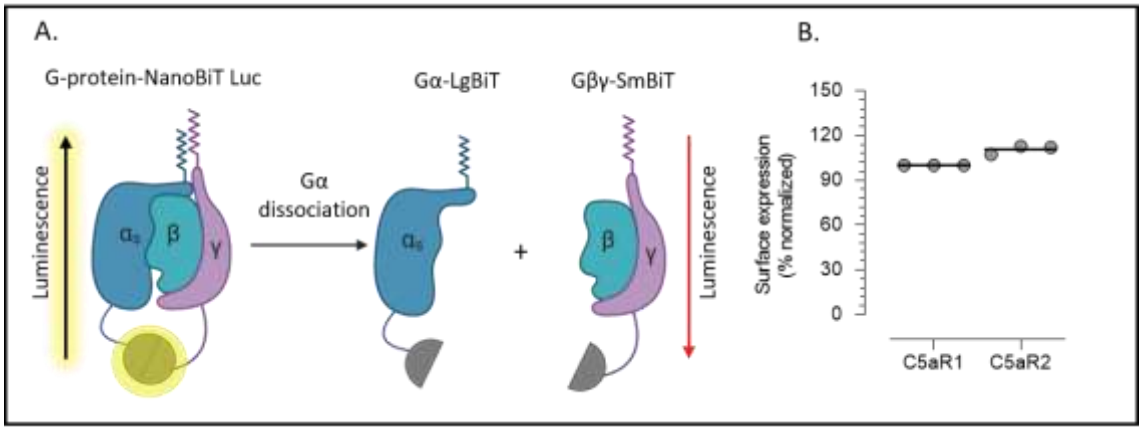

Figure 7 Measuring dissociation of heterotrimeric G proteins as a readout for G protein activation. **A.** Schematic representation of NanoBiT enzyme complementation assay to measure G protein dissociation. **B**. Surface expression of C5aR1 and C5aR2 constructs used in G-protein dissociation assay as measured by flow cytometry using an anti-FLAG primary antibody and AlexaFluor-488-coupled secondary antibody. Mean fluorescence intensity (MFI) values from nearly 20,000 cells per sample were used for analysis *(Adapted from Pandey S. et al., bioRxiv, 2021)* [37].

The agonist-induced change in luminescent signal arising from the dissociation of Gα and Gβγ sub-units was measured as a readout of G-protein activation [18]. C5aR1 was used as the prototypical counterparts of C5aR2, respectively. We observed that while agonist stimulation of C5aR1 resulted in robust activation of the Gαi subtype as expected, C5aR2 failed to cause the dissociation of any of the Gαi/o family proteins (Figure 8 A-D).

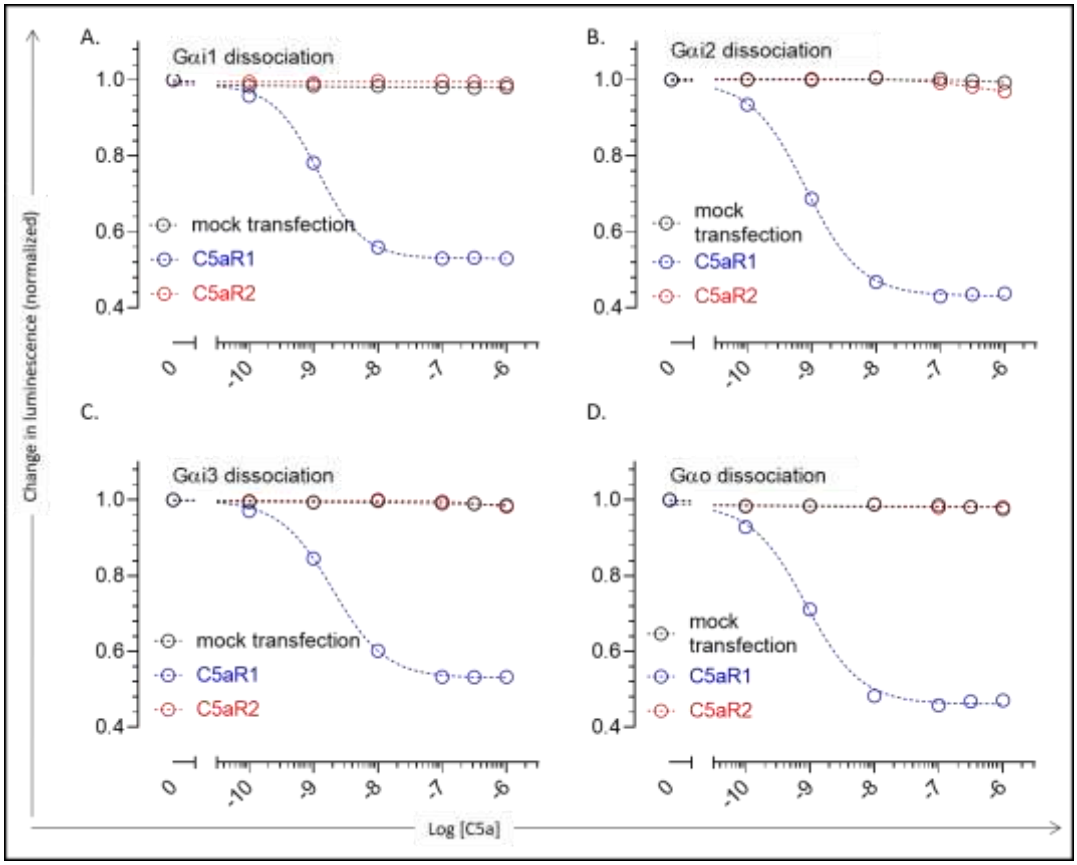

Figure 8 C5aR2 does not activate Gαi/o family of G proteins. A-D. Agonist-induced dissociation of heterotrimeric G proteins of Gαi/o family for C5aR1-C5aR2 receptor pair measured using NanoBiT assay. HEK-293 cells were transfected with the indicated receptor and Sm/Lg-BiT constructs of G-protein, i.e., Gαi1 (**A**), Gαi2 (**B**), Gαi3 (**C**) and Gαo (**D**) along with the,β,γ sub-units. The cells were stimulated with indicated concentrations of C5a, and the decrease in luminescence signal upon NanoBiT dissociation was measured as a readout of G-protein coupling. Data represent the mean ± SEM of three independent experiments, normalized with respect to baseline signal (i.e., vehicle treated) *(Adapted from Pandey S. et al., bioRxiv, 2021)* [37].

Similarly, we did not observe a decrease in luminescence for Gαs and Gαq upon C5a stimulation of the cells expressing either C5aR1 or C5aR2, indicating the inability of these receptors to activate Gαs and Gαq (Figure 9 A-B).

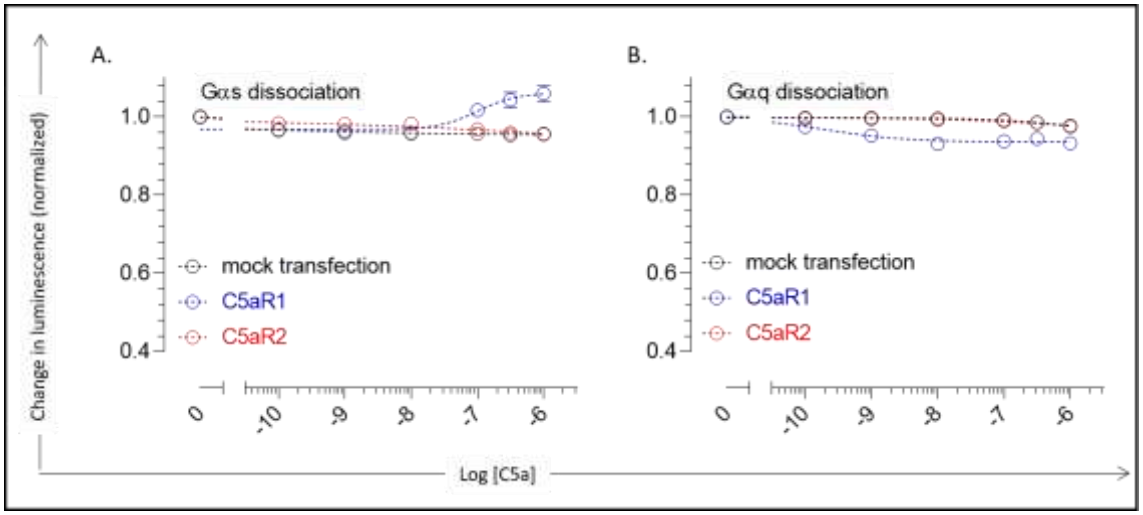

Figure 9 C5aR2 does not cause the dissociation of Gαs and Gαq. A-B. Agonist-induced dissociation of heterotrimeric G proteins of Gαs (**A**) and Gαq (**B**) family for C5aR1-C5aR2 receptor pair was measured using NanoBiT assay as mentioned above. Data were plotted as the mean ± SEM of three independent experiments and normalized with respect to baseline signal (i.e., vehicle treated) *(Adapted from Pandey S. et al., bioRxiv, 2021)* [37].

Interestingly, however, we noticed in case of C5aR2, when cells expressing $G\alpha_{12}$ were treated with C5a, there was a slight decrease in luminescence at higher C5a concentrations, indicating C5aR2 induced dissociation of $G\alpha_{12}$ for C5aR2 (Figure 10 A-B). However, additional experiments such as the assessment of physical association of $G\alpha_{12}$ with C5aR2 would be required to validate this further.

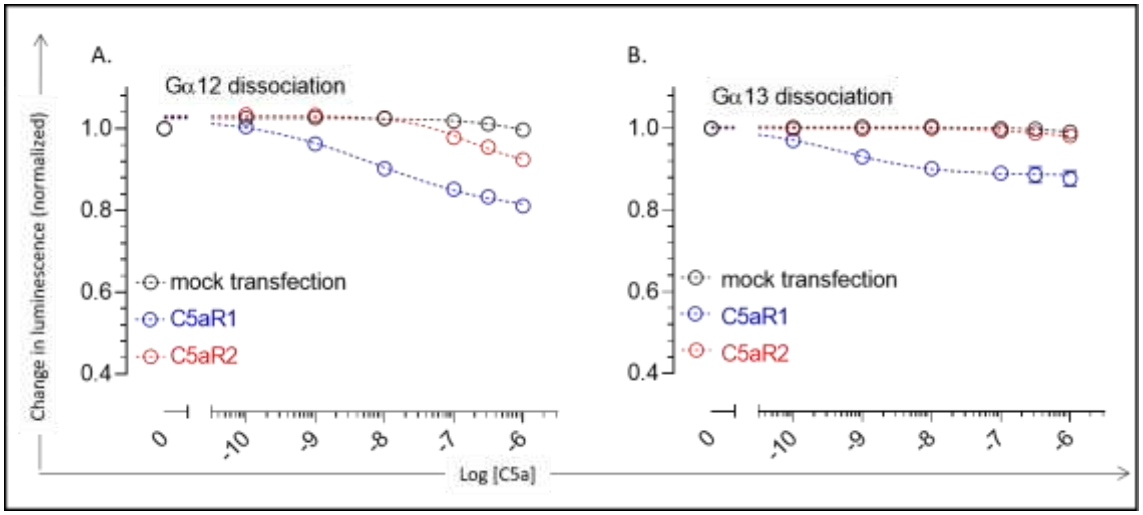

Figure 10 C5aR2 causes a slight dissociation of $G\alpha_{12}$ upon C5a stimulation. C5a-induced dissociation of heterotrimeric G proteins of $G\alpha_{12}$ (**A**) and $G\alpha_{13}$ (**B**) family for C5aR1 and C5aR2 was measured using NanoBiT assay as mentioned above. Data represent mean ± SEM of three independent experiments normalized with respect to baseline signal (i.e., vehicle treated) *(Adapted from Pandey S. et al., bioRxiv, 2021)* [37].

We also conducted a second messenger response assay to explore if agonist stimulation of C5aR2 results in a downstream signaling response. Since C5aR1, the prototypical GPCR is a Gαi coupled receptor; we assessed the functional coupling of C5aR2 with Gαi by measuring the agonist induced cAMP depletion using GloSensor assay. Similar to the previous experiment, we discovered that C5aR2 also failed to elicit any detectable second messenger response in cAMP assay while C5aR1 exhibited the expected profile of Gαi (Figure 11A). In our laboratory, we also measured the second messenger responses for Gαs and Gαq, and we observed that C5aR2 failed to induce a second messenger response for these G proteins as well [38,37] (Figure 11B). Collectively, these data demonstrate the absence of measurable activation of common G-proteins upon agonist-stimulation of C5aR2. However, an interesting question that remains to be explored is whether C5aR2 lacks a physical interaction with G-proteins or is incapable of activating G-proteins despite a physical interaction. In the future, the studies aimed at investigating the physical interaction of C5aR2 with heterotrimeric G proteins would provide invaluable information about the incapability of C5aR2 to signal through G proteins.

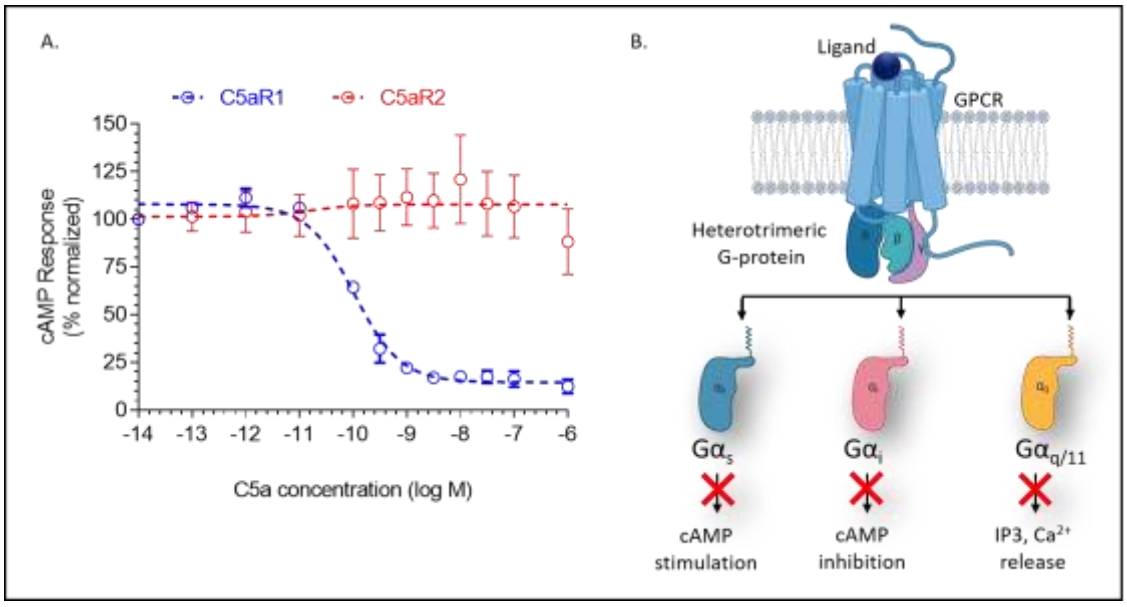

Figure 11 C5aR2 lacks functional G protein coupling. A. C5a induced inhibition of cAMP response was measured using GloSensor assay as a readout for Gαi coupling to C5aR2. HEK-293 cells expressing either C5aR1 or C5aR2 at similar levels were used for this assay, and cAMP response was measured using the standard protocol described in the method section. Data were normalized with respect to minimum C5a concentration (treated as 100%) and represent mean ± SEM of two independent experiments. **B.** C5aR2 fails to initiate a second messenger response for all the three major G protein subtypes.

Agonist stimulation of C5aR2 induces βarrestin recruitment and trafficking

In order to assess βarr-recruitment to C5aR2, we first used a co-immunoprecipitation assay by overexpressing C5aR2 in HEK-293 cells followed by agonist-stimulation, the addition of purified βarrs,

and chemical cross-crosslinking with DSP. We observed βarr1 and 2 robustly interacted with each of these receptors upon agonist-stimulation (Figure 12 B). We also performed the co-IP of βarr1 and 2 with C5aR2 by co-expressing βarrs with C5aR2 in HEK-293 cells, and we found a similar interaction of C5aR2 with both βarr1 and βarr2 (Figure 12 A), as observed in the previous case. In order to further confirm the interaction of C5aR2 with βarr, we reconstituted a complex of C5aR2 and βarr1, which was stabilized *In vitro* by a previously characterized synthetic antibody fragment (Fab30) directed against βarr1. The complex was further visualized by single-particle negative staining-based visualization by electron microscopy. As shown in Figure 12 C, we observed several 2D class-averages which resembled the previously described tail-engaged receptor-βarr interaction [39], which further confirms a direct interaction between C5aR2 and βarr1.

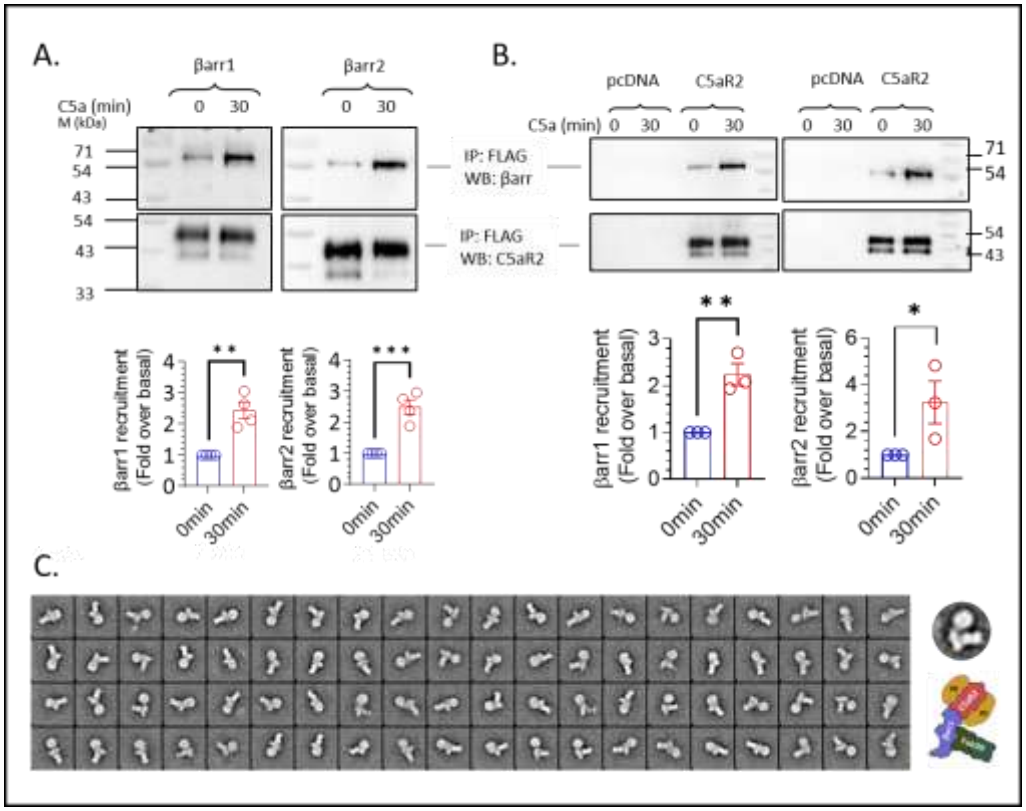

Figure 12 C5aR2 robustly recruits βarrs upon agonist stimulation. A. HEK-293 cells co-expressing the C5aR2 with either βarr1 or βarr2 were stimulated with C5a(100nM) followed by chemical cross-linking of C5aR2-βarr and co-IP using anti-Flag M1 antibody agarose. Receptors and βarrs were visualized by Western blot using the anti-βarr and anti-FLAG antibodies and quantified by densitometry. The bar graphs represent densitometry-based quantification of four independent experiments plotted as mean ± SEM and analyzed using Unpaired t-test (**p<0.01; ***p<0.001). **B.** HEK-293 cells expressing the indicated receptor constructs were stimulated with agonist, lysed, and incubated with purified βarr1/2, followed by co-IP of βarrs as mentioned in A. A representative blot from three independent experiments is shown here. The bar graphs represent densitometry-based quantification plotted as mean ± SEM and analyzed using Unpaired t-test (*p<0.05; **p<0.01). **C.** Visualization of C5aR2-βarr1 interaction by single particle electron microscopy. *Sf*9 cells expressing C5aR2, GRK2^{CAAX,} and βarr1 were stimulated with C5a (100 nM), stabilized using Fab30, followed by affinity purification of the

complex on anti-Flag M1 column. The complex was subjected to size-exclusion chromatography followed by negative staining based single particle analysis. 2D-class averages created from nearly ten thousand particles are shown here, and a typical 2D class average is indicated together with a schematic representation of the complex *(Adapted from Pandey S. et al., bioRxiv, 2021)* [37].

We next visualized agonist-induced trafficking of mYFP-tagged βarr1 and 2 for C5aR1 C5aR2 using confocal microscopy, and we detected that both of these receptors exhibited a typical "class B" pattern of βarr trafficking as reported previously for other GPCRs [40]. Upon agonist-stimulation, βarrs were first localized to the membrane, followed by their trafficking to endosomal vesicles (Figure 12 A) with an apparent preference for βarr2 in the case of C5aR2 (Figure 12 A-C). Surprisingly, we also observed some level of constitutive βarr localization to the plasma membrane in C5aR2 expressing cells even in the absence of agonist stimulation which was more prominent for βarr2 (Figure 12 A-C). We further corroborated agonist-induced trafficking of βarr1 and 2 and their basal recruitment to the receptor by using mCherry-tagged βarr1/2 constructs in confocal microscopy (Figure 12 B) and scoring βarr1/2 localization patterns from a pool of cells (Figure 12 C).

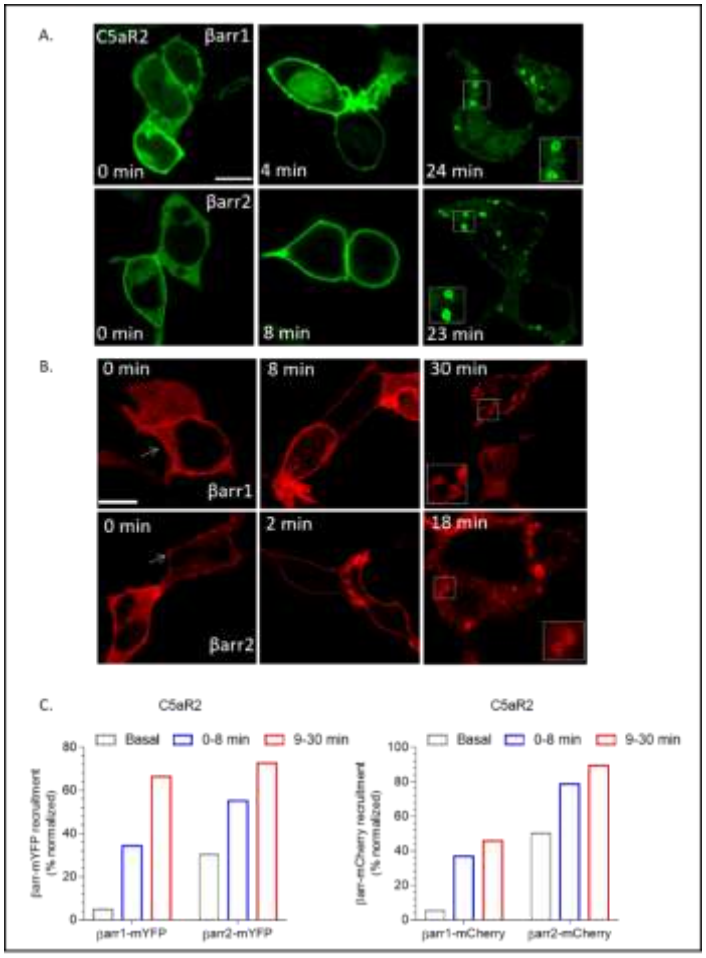

Figure 12 C5a stimulation induces trafficking of βarrs to endosomes. A-B. Agonist-induced trafficking of βarrs was measured by live cell confocal microscopy in HEK-293 cells expressing C5aR2 and either mYFP-tagged βarrs(as shown in **A**) or mcherry-tagged βarrs (shown in **B**). The cells were stimulated

with C5a(100 nM), and trafficking of βarrs was monitored at indicated time points. Representative images from three independent experiments are shown (scale bar is 10µm). There is some basal recruitment of βarrs, as can be seen in A and B. **C.** Quantification of agonist-induced βarr translocation in C5aR2 expressing cells measured by confocal microscopy. βarr localization at the cell surface and in punctate structures (endosomal vesicles) was scored under basal and stimulated conditions at indicated time points as a readout of βarr recruitment. The images were grouped into three classes, i.e., 0min, 1-8min, and 9-30min after stimulation to reflect basal, early, and late time-frames, respectively. Approximately five hundred cells from three independent experiments were counted for each condition, and the graphs represent % of cells showing βarr recruitment (i.e., localization at the cell surface, in punctate structures, or both) *(Adapted from Pandey S. et al., bioRxiv, 2021)* [37]

GRK5/6 are the primary determinants of βarr recruitment to C5a receptors

As discussed in the previous section, GPCR phosphorylation mediated by GRKs is a crucial determinant for βarr recruitment and downstream signaling. Therefore, we assessed the role of distinct GRK isoforms from two different GRK subfamilies in driving agonist-induced βarr recruitment by performing NanoBiT based βarr recruitment assay (Figure 13 A). We exploited the recently generated CRISPR-CAS9 based GRK knock-out cell lines [23]. We performed βarr recruitment assays under Gαi/Gαo-inhibited conditions by co-expressing the catalytic subunit of pertussis toxin (PTX) to compare the responses for each of the receptors in the absence of G-protein signaling. We observed that both C5aR1 and C5aR2 primarily depend on GRK5/6 for βarr recruitment (Figure 13 B).

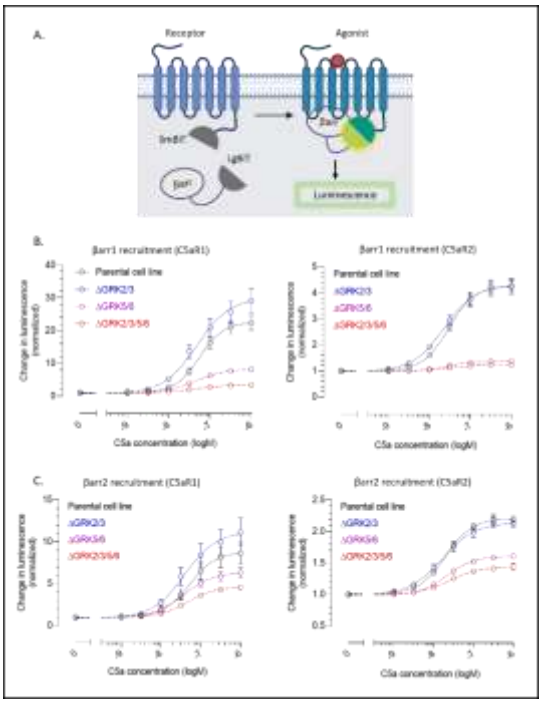

Figure 13 The agonist induced phosphorylation of C5aR1 and C5aR2 is GRK5/6 dependent. A. Schematic representation of agonist βarr1/2 recruitment using NanoBiT assay. **B-C.** Specific GRK knockout cell lines were transfected with C5aR1 or C5aR2 along with βarr1/2. The agonist-induced recruitment of either βarr1 (shown in B) or βarr2 (shown in C) in GRK-KO cell lines was measured using the NanoBiT assay. The data were normalized with respect to baseline signal (i.e., vehicle treated) and

plotted as mean ± SEM of three independent experiments *(Adapted from Pandey S. et al., bioRxiv, 2021)* [37].

Distinct conformational signatures of C5aR1 and C5aR2

Next, to probe if the distinct transducer-coupling preference of C5aR2 with respect to its canonical counterpart C5aR1 may impart distinct βarr conformations, we measured the conformational signatures of βarrs upon their interaction with these receptors. We first analyzed the conformations of βarr1 upon engagement with C5aR1 and C5aR2.To test our hypothesis, we used a previously described intrabody30 (Ib30)-based sensor for βarr1 (Figure 14 A), which selectively recognizes receptor-bound active conformation of βarr1, and reports agonist-induced formation of a receptor-βarr1 complex in cellular context [24,41]. We observed that under normalized surface expression conditions, the Ib30 sensor robustly recognized the conformation of βarr1 upon C5a-stimulation of C5aR1, but it failed to recognize the conformation of βarr1 bound to C5aR2 (Figure 14 B). As demonstrated in the previous section, C5aR2 very efficiently recruits βarr1 upon agonist stimulation, the lack of Ib30 sensor reactivity indicates a distinct conformation of C5aR2-bound βarr1 compared to C5aR1-bound βarr1.

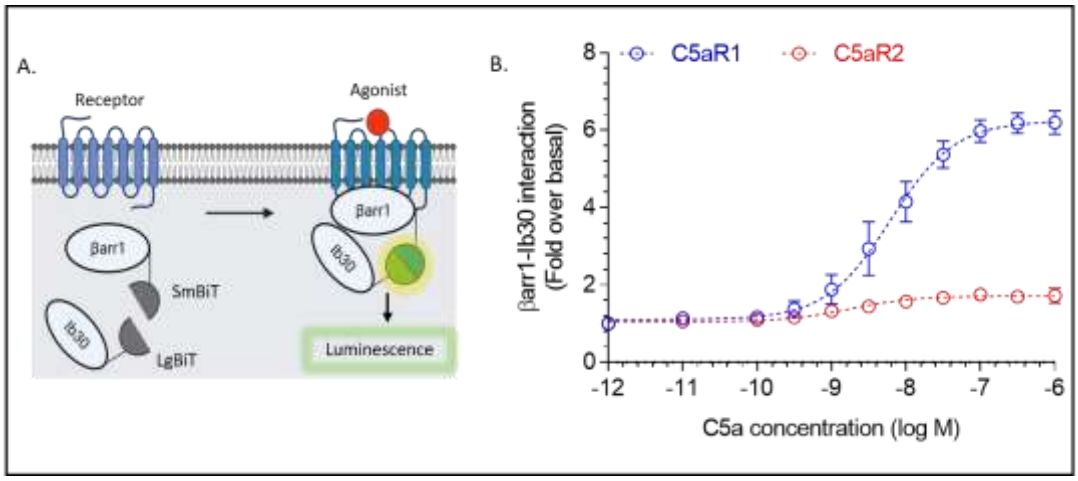

Figure 14 βarr1 adopts distinct conformations upon interaction with C5aR1 and C5aR2. A. Intrabody30-based (Ib30) conformational sensor developed in the NanoBiT format recognizes the active conformation of receptor-bound βarr1. **B.** HEK-293 cells expressing either C5aR1 or C5aR2 along with LgBiT-Ib30 and SmBiT-βarr1 were stimulated with indicated concentrations of the C5a, and an increase in luminescence signal was measured. Data were normalized with respect to the maximal response of C5aR1(at 1µM agonist concentration treated as 100%). Data represent mean ± SEM of four independent experiments *(Adapted from Pandey S. et al., bioRxiv, 2021)* [37].

Second, we also probed the conformations of βarr2 in complex with either C5aR1 or C5aR2 by employing FlAsH-BRET based sensors of βarr2 [25]. These intramolecular sensors contain a BRET donor (R-luciferase) at the N-terminus of βarr2 while FlAsH labeling sequences (tetracysteine motifs) at

different positions (Figure 15 A). Thus, a comparison of the change in the BRET signal for two different receptors can provide insights into the conformational signatures of βarr2. As presented in Figure 4.13 B, we observed a striking difference in the change in the BRET signal for the C5aR1-C5aR2 receptor pair. For example, there is a directionally opposite change in the BRET signal for the F6 sensor upon activation of C5aR1 vs. C5aR2 (Figure 15 B).

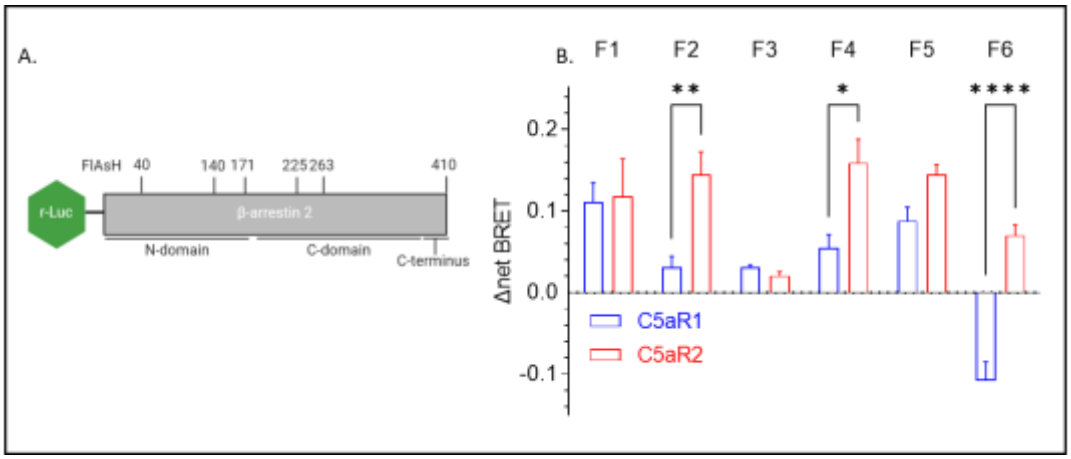

Figure 15 BRET based sensors of βarr2 conformational signatures reveal distinct conformational signatures of βarr2 between C5aR1 and C5aR2. **A**. The schematic representation of BRET based conformational sensor where βarr2 is tagged with r-Luc (Renilla luciferase) at N-terminus as BRET donor while FlAsH motif (as BRET acceptor) is encoded in various positions in βarr2. **B.** HEK-293 cells expressing either C5aR1 or C5aR2 and BRET sensors were labeled with FlAsH reagent followed by agonist-stimulation and measurement of BRET signal. Data were plotted as mean ± SEM of four independent experiments and analyzed using Two-Way ANOVA (*p<0.05, **p<0.01, ***p<0.001) *(Adapted from Pandey S. et al., bioRxiv, 2021)* [37].

Taken together, these data further corroborate the conformational differences in βarr1 revealed by the Ib30 sensor and collectively establish distinct βarr conformations induced by C5aR2 compared to its canonical counterpart, C5aR1. Although these assays are analytically quantitative, they do not directly reveal the exact differences in βarr conformations for these two receptors. In the future, high-resolution structural studies would be required to pinpoint and directly visualize the conformational difference of βarrs for these two receptors.

Expression of C5aR2 results in distinct ERK1/2 phosphorylation profile than C5aR1

Agonist-induced ERK1/2 MAP kinase phosphorylation is one of the most well-studied readouts of βarr dependent signaling, and therefore, we assessed whether the agonist stimulation of C5aR2 results in downstream ERK1/2 phosphorylation. Upon agonist stimulation, we observed a typical pattern of ERK1/2 phosphorylation for C5aR1; interestingly, we observed an elevated level of pERK1/2 in C5aR2 expressing cells, which was significantly reduced upon C5a-stimulation in a dose-dependent manner (Figure 16 A-B).

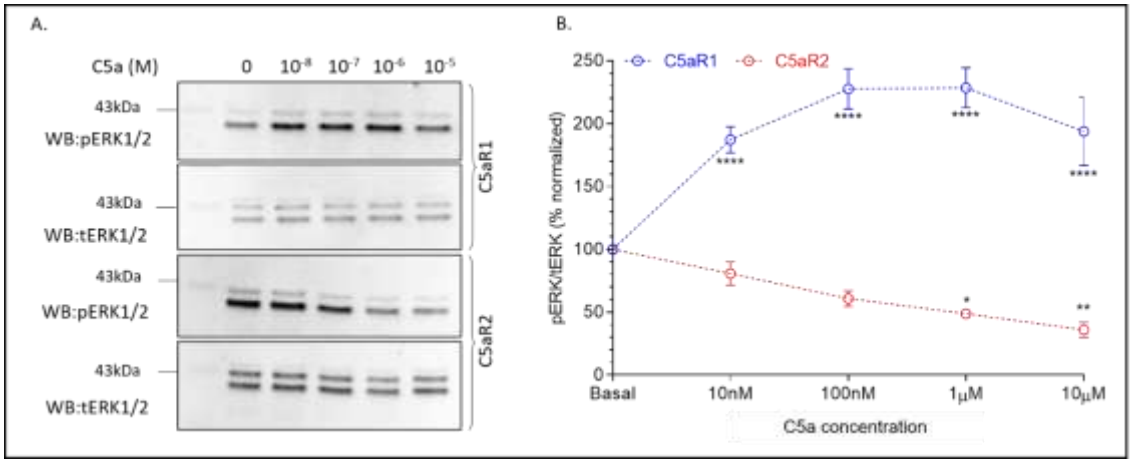

Figure 16 C5aR2 exhibits an atypical pattern of ERK1/2 phosphorylation. A. HEK-293 cells expressing C5aR1 exhibit a typical ERK1/2 phosphorylation pattern upon agonist-stimulation, while cells expressing C5aR2 display an enhanced level of basal ERK1/2 phosphorylation, which decreases upon C5a-stimulation. **B.** The data represent densitometric quantification of 5 experiments, plotted as mean ± SEM and analyzed using Two-Way ANOVA (****, p<0.0001) *(Adapted from Pandey S. et al., bioRxiv, 2021)* [37].

However, we observed that unlike C5aR1, the elevated level of phospho-ERK1/2 in case of C5aR2 was insensitive to PTX pre-treatment (i.e., Gαi inhibition) (Figure 17 A-B). This observation hints towards a distinct mode of ERK1/2 phosphorylation in the basal state in case of C5aR2.

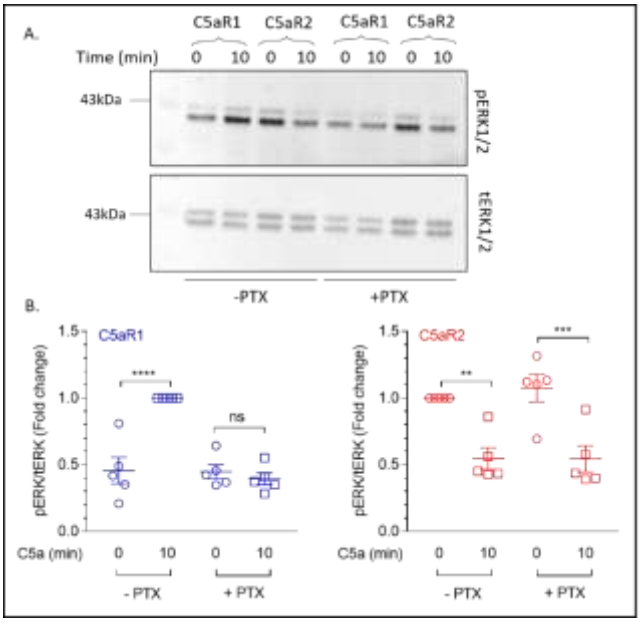

Figure 17 C5aR2 mediated basal ERK1/2 phosphorylation is insensitive to pertussis toxin treatment. A. PTX-treatment ablates C5a-induced ERK1/2 phosphorylation in C5aR1 expressing cells, but it does not affect the elevated level of basal ERK1/2 phosphorylation C5aR2 expressing cells. ERK1/2 phosphorylation was measured after PTX treatment, as mentioned previously. **B.** The data represent densitometric quantification of five independent experiments, plotted as mean ± SEM and analyzed using Two-Way ANOVA (**, p<0.01, ***p<0.001, ***p<0.0001) *(Adapted from Pandey S. et al., bioRxiv, 2021)* [37].

To investigate the possible mechanism of basal ERK1/2 phosphorylation in case of C5aR2, we treated the cells expressing either C5aR1 or C5aR2 with a pan MEK inhibitor U0126. Surprisingly, we observed that ERK1/2 phosphorylation was entirely ablated for both C5aR1 and C5aR2 with U0126 (MEK inhibitor) pre-treatment (Figure 18 A-B).

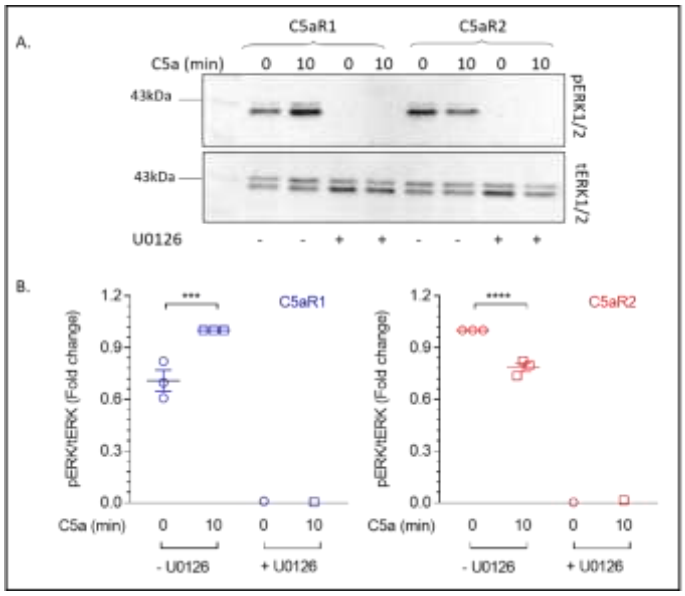

Figure 18 C5aR2 mediated basal ERK1/2 phosphorylation is sensitive to U0126 treatment. A. Treatment of cells with U0126, a pan MEK inhibitor, results in complete loss of ERK1/2 phosphorylation for both C5aR1 and C5aR2, suggesting the involvement of a canonical mechanism of ERK1/2 phosphorylation. **B**. The data represent densitometry based quantification of 3 independent experiments, plotted as mean ± SEM and analyzed using Two-Way ANOVA (***, p<0.001; ***p<0.0001) *(Adapted from Pandey S. et al., bioRxiv, 2021)* [37].

Taken together, our data suggest that the expression of C5aR2 results in an enhanced level of basal phosphor-ERK1/2. While a canonical pathway involving MEK may be involved in maintaining the enhanced basal phospho-ERK1/2, it is not dependent on Gαi. As mentioned earlier, we observed a measurable level of constitutive βarr localization in the membrane for C5aR2 expressing cells, and therefore, we also measured the effect of βarr knock-down on the basal level of ERK1/2 phosphorylation. Surprisingly, however, although the knock-down of βarr1 or 2 did not affect the elevated basal level of ERK1/2 phosphorylation in C5aR2 expressing cells, βarr2 depletion appears to reduce the effect of C5a on lowering ERK1/2 phosphorylation (Figure 19).

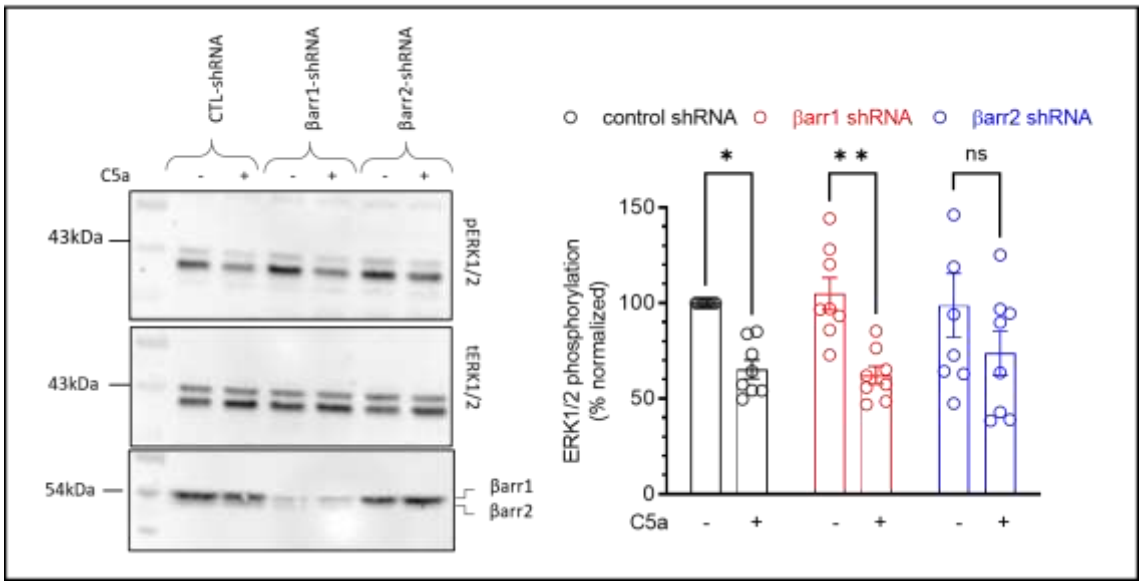

Figure 19 Effect of βarr depletion on ERK1/2 phosphorylation. βarr1/2 knockdown cells expressing C5aR2 were stimulated with C5a (100 nM) for indicated time points. The shRNA-mediated knockdown of βarr2 but not βarr1 attenuates the C5a-induced lowering of pERK1/2 while knockdown of either βarrs have no significant effect on basal pERK1/2. The data on the right panel show the densitometry-based quantification from eight independent experiments (plotted as mean ± SEM) and normalized with respect to the basal pERK1/2 under control shRNA conditions (One-Way ANOVA, *p<0.05; **p<0.01) *(Adapted from Pandey S. et al., bioRxiv, 2021)* [37].

Our findings indicate that as C5aR2 does not exhibit the prototypical ERK1/2 phosphorylation pattern, it may have a modulatory role in C5aR1 induced ERK1/2 activation. However, additional studies would be required to understand the precise role of C5aR2 in ERK1/2 phosphorylation and uncover the mechanistic basis of this intriguing observation in detail.

C5aR2 activation by C5a mediates p90RSK phosphorylation

To explore the potential signaling pathways downstream of C5aR2, we performed a phospho-antibody array-based screen to identify cellular proteins that exhibit a change in their phosphorylation status upon C5a stimulation of either C5aR1 or C5aR2. We observed that several proteins undergo phosphorylation/dephosphorylation upon stimulation of C5aR1 and C5aR2 expressing stable cell lines, and interestingly, some of the proteins were common to both receptors, implying a potential role of βarrs in activation of downstream signaling for C5aR2 (Figure 20).

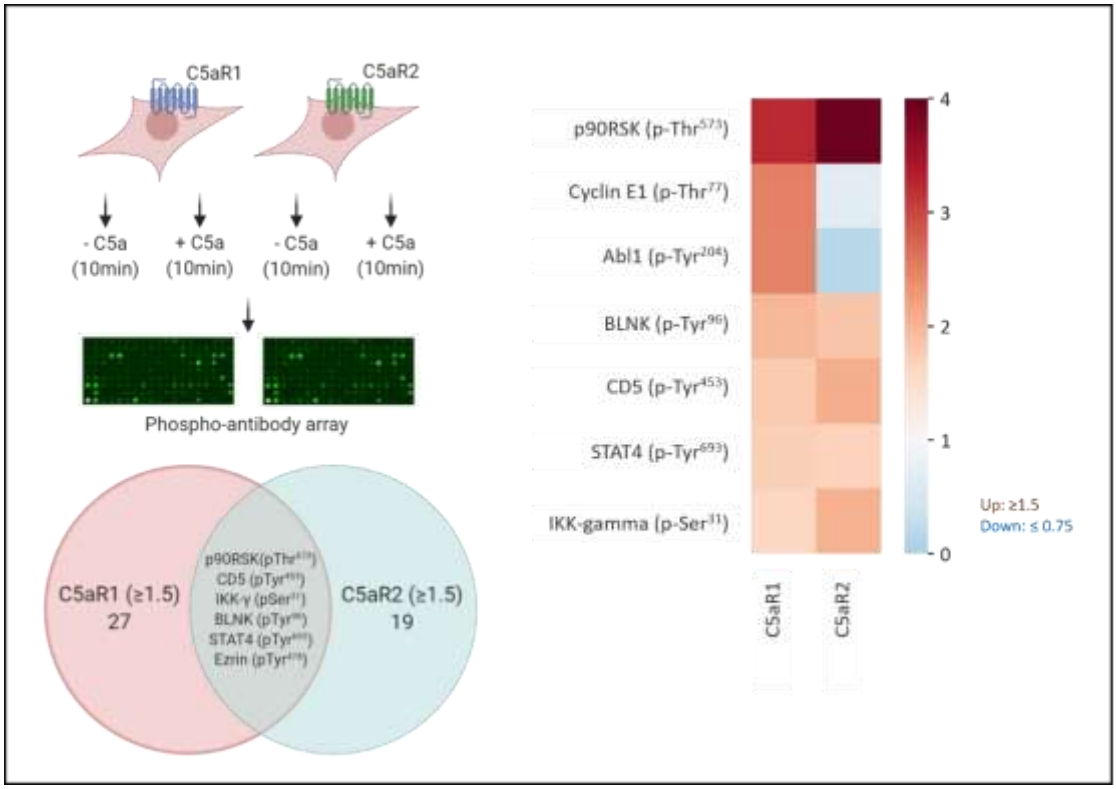

Figure 20 Identification of potential signaling pathways downstream of C5aR2. Phospho-antibody array on HEK-293 cells stably expressing C5aR1 or C5aR2 reveals a change in the phosphorylation status of various cellular proteins, some of which are common to both C5aR1 and C5aR2. The signal ratios of these proteins were analyzed after phosphoprotein detection using phospho-antibody array. Of these, a ribosomal kinase p90RSK displayed the maximum signal ratio both for C5aR1 and C5aR2 after agonist stimulation *(Adapted from Pandey S. et al., bioRxiv, 2021)* [37].

We experimentally validated agonist-induced phosphorylation of one of these proteins, p90RSK, at three distinct phosphorylation sites, namely Thr^{359}, $Ser^{380,}$ and $Thr^{573,}$ in different cellular contexts. We discovered that C5a stimulation of C5aR2 expressing cells resulted in time-dependent phosphorylation p90RSK at Ser^{380} (Figure 21 A); the phosphorylation data for the other two sites (Thr^{359} and Thr^{573}) was not consistent. Interestingly, we noticed that C5a-induced phosphorylation of p90RSK at Ser^{380} was significantly reduced upon βarr1 knock-down in HEK-293 cells suggesting a potential involvement of βarr1 (Figure 21 B).

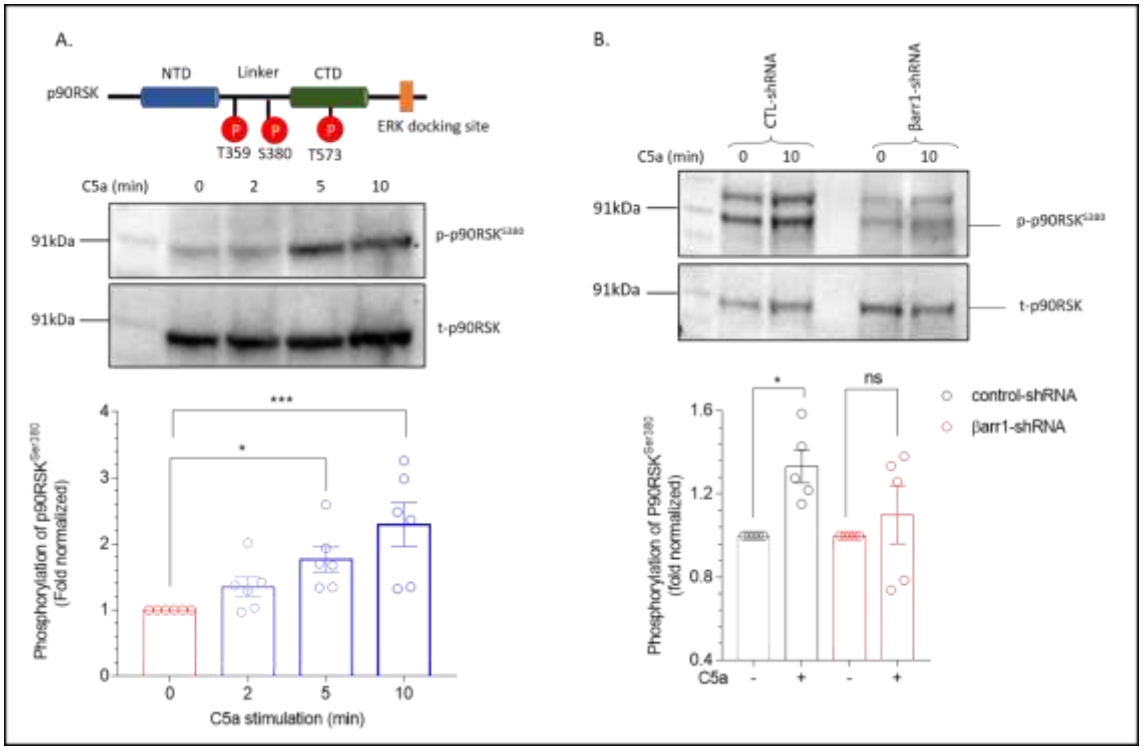

Figure 21 p90RSK exhibits robust agonist dependent phosphorylation in βarr1 dependent fashion. A. C5a stimulation of HEK-293 cells expressing C5aR2 results in robust phosphorylation of p90RSK at the endogenous level. The cellular lysates were probed for p90RSK using phosphosite specific antibodies by Western blotting. The data shown in the lower-left panel represent the densitometry-based quantification of six independent experiments plotted as mean ± SEM and analyzed using One-way ANOVA(*p<0.05, ***p<0.001). **B.** C5a-induced p90RSK phosphorylation is βarr1 dependent as detected by the knock-down of βarr1 in HEK-293 cells. The knockdown of βarr1 lowers p90RSK phosphorylation compared to control. The phosphoprotein detection was performed as mention above. The data shown in the lower-right panel represents densitometry-based quantification of five independent experiments plotted as mean ± SEM) is presented (**p<0.01; One-Way ANOVA) *(Adapted from Pandey S. et al., bioRxiv, 2021)* [37].

In order to further corroborate our findings, we measured C5a-induced p90RSK phosphorylation in human monocyte-derived macrophages (HMDMs) using an *in-cell ELISA* approach. HMDMs express both the receptors, i.e., C5aR1 and C5aR2, at an endogenous, although efficient knock-down of βarrs in primary cells is technically challenging. Therefore, we used a pharmacological approach to dissect the specific contribution of C5aR2 by using a C5aR2-specific agonist (P32) [42]. As shown in Figure 4.22 A, we observed that C5a stimulation of HMDMs led to robust p90RSK phosphorylation at $Thr^{573,}$ and this was identical to the phosphorylation induced by P32. Interestingly, pre-treatment of these cells with a C5aR1 specific antagonist (PMX53) [26] did not affect P32-induced p90RSK phosphorylation suggesting that the phosphorylation of p90RSK at the Thr^{573} site is indeed mediated through C5aR2 (Figure 22 A). In contrast, C5a-induced phosphorylation of Thr^{359} and Ser^{380} in HMDMs appears to be mediated primarily by C5aR1 as pre-treatment with PMX53 nearly blocked C5a response, and stimulation with P32 alone failed to yield a significant response (Figure 4.22 B-C).

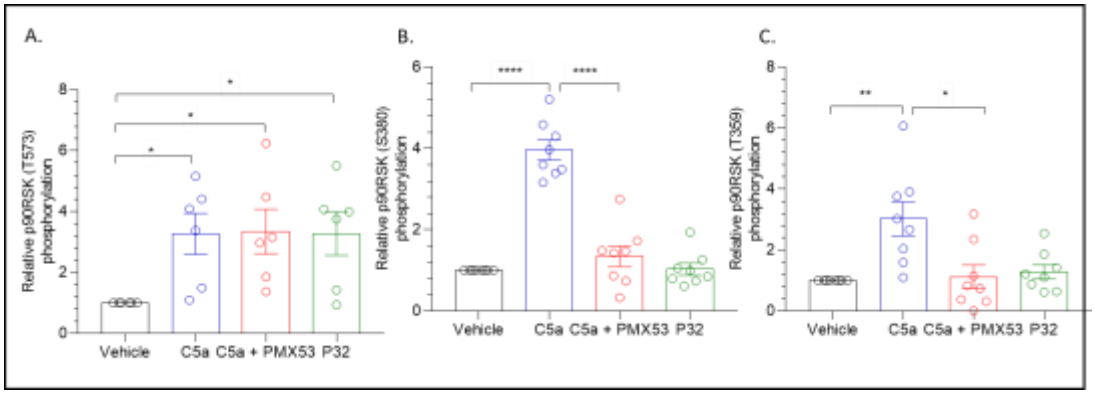

Figure 22 Agonist-induced p90RSK phosphorylation in HMDMs. A. Stimulation of HMDMs with either C5a or P32 (a C5aR2-selective agonist) results in robust phosphorylation p90RSK at Thr573. Moreover, the C5aR1-selective antagonist, PMX53, does not block p90RSK phosphorylation at this site, suggesting that it is mediated by C5aR2. **B-C.** The phosphorylation of p90RSK at Ser380 and Thr359 are primarily mediated through C5aR1 activation as pre-treatment with PMX53 blocks C5a-induced response. Furthermore, P32 stimulation also fails to induce significant phosphorylation on these sites. p90RSK phosphorylation at indicated sites was measured using *in-cell ELISA* method with corresponding antibodies as mentioned in the methods section. Experiments were performed in HMDMs derived from eight different donors. The data were plotted as mean ± SEM and normalized with respect to vehicle-treated conditions. The analysis was done using Fisher's LSD test (*p<0.05, **p<0.01, ****p<0.0001), assuming each treatment group is independent of each other - only donors with a >1 response to C5a are included *(Adapted from Pandey S. et al., bioRxiv, 2021)* [37].

STATISTICAL ANALYSIS:

All the experiments were conducted at least three times and data were plotted and analyzed using GraphPad Prism software (Prism 8.0). Heat maps were plotted in Python 3.7 using appropriate libraries. The data were normalized with respect to proper experimental controls and appropriate statistical analyses were performed.

DISCUSSION:

In conclusion, we have discovered $C5a^{pep}$ as a biased C5aR1 agonist at the levels of $G\alpha_i$ *versus* βarr recruitment, signaling outcomes, and cellular responses. Going forward, an interesting direction might be to assess the physiological responses induced by $C5a^{pep}$ *in vivo*. Given that C5a attenuates LPS-mediated IL-6 production from macrophages[34] (Figure 2.13A), a biased ligand such as $C5a^{pep}$ that retains this beneficial activity, although with weaker pro-inflammatory activities, may be exploited as a novel tool to design therapeutics aimed at treating inflammatory disorders. Furthermore, as we have shown the recruitment of both isoforms of βarr (*i.e.,* βarr1 and 2) to C5aR1, it would be enticing to understand the precise roles of these βarr isoforms in the regulation of signaling through C5aR1.

Moreover, our study highlights the divergence in the behavior of two different receptors of the complement system, C5aR1, and C5aR2. The NanoBiT-based G-protein dissociation assay and second messenger assays demonstrate the lack of common G-protein coupling upon activation of C5aR2. In this context, it would be tantalizing to explore whether C5aR2 undergoes an activation-dependent conformational change similar to that observed for prototypical GPCRs, including an outward movement of transmembrane (TM) helix 5 and 6 [4]. It is plausible that activation-dependent outward movement of TM5 and TM6 is restricted in the case of C5aR2, which does not permit G-protein interaction; however, exploring this possibility requires additional studies. While structural elucidation of GPCR activation and signaling has seen exponential progress, direct structural analysis C5aR2 is still somewhat limited and requires additional efforts going forward.

C5aR2 has remained a mysterious receptor since its discovery due to unusual behavior in terms of lack of G-protein activation and downstream signaling. It has been shown previously to be involved in broadly modulating GPCR signaling, including that of C5aR1 [26,43]; however, direct involvement of C5aR2 in initiating a signaling pathway has not been established yet. We observed an enhanced level of basal ERK1/2 phosphorylation in HEK-293 cells expressing C5aR2, which is reduced upon C5a-stimulation, but it was insensitive to Gαi inhibition or βarr depletion. Notably, we also discovered that several cellular proteins, including p90RSK, demonstrated a change in their phosphorylation status upon C5aR2 activation. Interestingly, the agonist induced phosphorylation of p90RSK downstream of C5aR2 was sensitive to βarr1 depletion. Therefore, our study provides a framework for exploring additional signaling pathways downstream of C5aR2 and may help uncover novel functions of C5aR2 going forward. The interplay of G-proteins and βarrs in ERK1/2 MAP kinase activation downstream of GPCRs has recently emerged as an exciting paradigm [44,45,46]. In this context, our data underscore two interesting points. First, the recruitment of βarrs to 7TMRs may not necessarily translate to ERK1/2 activation, and second, there may exist receptor-specific fine-tuning of this interplay. Our findings establish C5aR2, together with its prototypical GPCR counterpart C5aR1, as a fascinating system to further probe the mechanistic interplay of G-proteins and βarrs in ERK1/2 activation.

Distinct binding modes and conformations of βarrs have emerged as the primary mechanism driving their multifunctionality and functional diversity [47–49]. Recent structures of GPCR-arrestin complexes have also revealed distinct orientation of arrestins in complex with different receptors [50–53]. For example, a comparison of the rhodopsin-visual-arrestin structure with the neurotensin receptor-βarr1 complex reveals a large rotation of βarr1 in the plane of the membrane, which is not apparent in the M2R-βarr1 and β_1AR-βarr1 structures [54]. Distinct conformational states of βarrs upon their interaction with C5aR2 compared to C5aR1 observed in the current study further underscore the

conformational diversity in 7TMR-βarr interaction. Our work with the non-canonical 7TMR, C5aR2, provides a new handle to link conformational signatures in βarrs to specific functional outcomes.

In summary, our study establishes C5aR2 as a bona fide "arrestin-coupled receptor" with a lack of detectable G-protein coupling and potential signaling through non-canonical pathways. Moreover, we also establish that βarrs adopt distinct conformations upon interaction with these receptors than prototypical GPCRs, which underscores the conformational diversity of 7TMR-βarr complexes. Our findings underscore distinct functional capabilities of 7TMRs, and they have broad implications to better understand the framework of biased agonism at these receptors.

IMPACT OF THE RESEARCH IN THE ADVANCEMENT OF KNOWLEDGE OR BENEFIT OF MANKIND:

The Complement C5a receptor belongs to the GPCR superfamily, which are the targets to nearly one third of the currently marketed drugs. These two receptors are known to be involved in several autoimmune and inflammatory diseases. Currently, the study of GPCRs has witnessed a revolutionizing phenomenon of biased signaling, where it has become possible to design ligands or drugs that selectively target one signaling pathway over the other, and such ligands are known as biased ligands. The advent of biased signaling has opened new avenues for designing therapeutic agents with reduced off-target effects and improved efficacy. Our study has established for the first time that biased receptors naturally exist in human body, which can be targeted for designing highly selective pathway specific drugs for several inflammatory disorders. We have also discovered a functionally selective ligand which can be leveraged to overcome the C5a induced hyperinflammation. Recent studies have demonstrated that when C5a binds to C5aR1, for example in COVID19 patients, a whole cascade of cellular signaling events are triggered, leading to excessive release of small cytokine proteins in the blood stream – a situation known as "cytokine storm" and excessive inflammation of tissues and organs. Scientists are trying to block this connection of C5a and C5aR1 using monoclonal antibodies – a specific type of proteins released by our immune system, to treat COVID19 patients. The discovery of working mechanisms of C5aR2 and D6R now provides an additional opportunity for therapeutic targeting.

LITERATURE REFERENCES:

1. Pierce, K. L., Premont, R. T. & Lefkowitz, R. J. Seven-transmembrane receptors. *Nat. Rev. Mol. Cell Biol.* **3**, 639–650 (2002).
2. Rosenbaum, D. M., Rasmussen, S. G. F. & Kobilka, B. K. The structure and function of G-protein-coupled receptors. *Nature* **459**, 356–363 (2009).
3. Reiter, E., Ahn, S., Shukla, A. K. & Lefkowitz, R. J. Molecular Mechanism of β-Arrestin-Biased Agonism at Seven-Transmembrane Receptors. *Annu. Rev. Pharmacol. Toxicol.* **52**, 179–197 (2012).

4. Weis, W. I. & Kobilka, B. K. The Molecular Basis of G Protein–Coupled Receptor Activation. *Annu. Rev. Biochem.* **87**, 897–919 (2014).
5. Rajagopal, S. *et al.* β-Arrestin- But not G protein-mediated signaling by the 'decoy' receptor CXCR7. *Proc. Natl. Acad. Sci. U. S. A.* **107**, 628–632 (2010).
6. Smith, J. S., Lefkowitz, R. J. & Rajagopal, S. Biased signalling : from simple. *Nat. Publ. Gr.* **17**, 243–260 (2018).
7. Scola, A.-M., Johswich, K.-O., Morgan, B. P., Klos, A. & Monk, P. N. The human complement fragment receptor, C5L2, is a recycling decoy receptor. *Mol. Immunol.* **46**, 1149–1162 (2009).
8. Ulvmar, M. H., Hub, E. & Rot, A. Atypical chemokine receptors. *Exp. Cell Res.* **317**, 556–568 (2011).
9. Borroni, E. M. *et al.* β-Arrestin–Dependent Activation of the Cofilin Pathway Is Required for the Scavenging Activity of the Atypical Chemokine Receptor D6. *Sci. Signal.* **6**, ra30–ra30 (2013).
10. Nibbs, R. J. B. & Graham, G. J. Immune regulation by atypical chemokine receptors. *Nat. Rev. Immunol.* **13**, 815–829 (2013).
11. Kalant, D. *et al.* C5L2 Is a Functional Receptor for Acylation-stimulating Protein*. *J. Biol. Chem.* **280**, 23936–23944 (2005).
12. Schatz-Jakobsen, J. A. *et al.* Structural and functional characterization of human and murine C5a anaphylatoxins. *Acta Crystallogr. D. Biol. Crystallogr.* **70**, 1704–1717 (2014).
13. Siciliano, S. J. *et al.* Two-site binding of C5a by its receptor: an alternative binding paradigm for G protein-coupled receptors. *Proc. Natl. Acad. Sci. U. S. A.* **91**, 1214–1218 (1994).
14. Pandey, S. *et al.* Partial ligand-receptor engagement yields functional bias at the human complement receptor, C5aR1. *J. Biol. Chem.* **294**, 9416–9429 (2019).
15. Konteatis, Z. D. *et al.* Development of C5a receptor antagonists. Differential loss of functional responses. *J. Immunol.* **153**, 4200–5 (1994).
16. Kawai, M. *et al.* Structure-function studies in a series of carboxyl-terminal octapeptide analogs of anaphylatoxin C5a. *J. Med. Chem.* **35**, 220–223 (1992).
17. Kumari, P., Dwivedi, H., Baidya, M. & Shukla, A. K. Measuring agonist-induced ERK MAP kinase phosphorylation for G-protein-coupled receptors. *Methods Cell Biol.* **149**, 141–153 (2019).
18. Inoue, A. *et al.* Illuminating G-Protein-Coupling Selectivity of GPCRs. *Cell* **177**, 1933-1947.e25 (2019).
19. Peisley, A. & Skiniotis, G. 2D Projection Analysis of GPCR Complexes by Negative Stain Electron Microscopy BT - G Protein-Coupled Receptors in Drug Discovery: Methods and Protocols. in (ed. Filizola, M.) 29–38 (Springer New York, 2015). doi:10.1007/978-1-4939-2914-6_3.
20. Tang, G. *et al.* EMAN2: An extensible image processing suite for electron microscopy. *J. Struct. Biol.* **157**, 38–46 (2007).
21. Yang, Z., Fang, J., Chittuluru, J., Asturias, F. J. & Penczek, P. A. Iterative Stable Alignment and Clustering of 2D Transmission Electron Microscope Images. *Structure* **20**, 237–247 (2012).
22. Moriya, T. *et al.* High-resolution single particle analysis from electron cryo-microscopy images using SPHIRE. *JoVE (Journal Vis. Exp.* e55448 (2017).
23. Arveseth, C. D. *et al.* Smoothened transduces Hedgehog signals via activity-dependent sequestration of PKA catalytic subunits. *PLOS Biol.* **19**, e3001191 (2021).
24. Baidya, M. *et al.* Key phosphorylation sites in GPCR s orchestrate the contribution of β-Arrestin 1 in ERK 1/2 activation. *EMBO Rep.* **21**, e49886 (2020).
25. Lee, M.-H. *et al.* The conformational signature of β-arrestin2 predicts its trafficking and signalling functions. *Nature* **531**, 665–668 (2016).
26. Li, X. X., Clark, R. J. & Woodruff, T. M. C5aR2 Activation Broadly Modulates the Signaling and Function of Primary Human Macrophages. *J. Immunol.* **205**, 1102 LP – 1112 (2020).
27. Li, X. X. *et al.* Pharmacological characterisation of small molecule C5aR1 inhibitors in human

cells reveals biased activities for signalling and function. *Biochem. Pharmacol.* 114156 (2020) doi:10.1016/j.bcp.2020.114156.
28. Kumar, B. A., Kumari, P., Sona, C. & Yadav, P. N. Chapter 2 - GloSensor assay for discovery of GPCR-selective ligands. in *G Protein-Coupled Receptors Part A* (ed. Shukla, A. K. B. T.-M. in C. B.) vol. 142 27–50 (Academic Press, 2017).
29. Croker, D. E., Halai, R., Fairlie, D. P. & Cooper, M. A. C5a, but not C5a-des Arg, induces upregulation of heteromer formation between complement C5a receptors C5aR and C5L2. *Immunol. Cell Biol.* **91**, 625–633 (2013).
30. Braun, L. & Christophe, T. Phosphorylation of Key Serine Residues Is Required for Internalization of the Complement 5a (C5a) Anaphylatoxin Receptor via a □ -Arrestin , Dynamin , and Clathrin-dependent Pathway *. **278**, 4277–4285 (2003).
31. Ranjan, R., Dwivedi, H., Baidya, M., Kumar, M. & Shukla, A. K. Novel Structural Insights into GPCR–β-Arrestin Interaction and Signaling. *Trends Cell Biol.* **27**, 851–862 (2017).
32. Srivastava, A., Gupta, B., Gupta, C. & Shukla, A. K. Emerging Functional Divergence of β-Arrestin Isoforms in GPCR Function. *Trends Endocrinol. Metab.* **26**, 628–642 (2015).
33. Sumichika, H. *et al.* Identification of a Potent and Orally Active Non-peptide C5a Receptor Antagonist*. *J. Biol. Chem.* **277**, 49403–49407 (2002).
34. Seow, V. *et al.* Inflammatory Responses Induced by Lipopolysaccharide Are Amplified in Primary Human Monocytes but Suppressed in Macrophages by Complement Protein C5a. *J. Immunol.* **191**, 4308 LP – 4316 (2013).
35. Klos, A., Wende, E., Wareham, K. J. & Monk, P. N. International Union of Basic and Clinical Pharmacology. LXXXVII. Complement Peptide C5a, C4a, and C3a Receptors. *Pharmacol. Rev.* **65**, 500 LP – 543 (2013).
36. Okinaga, S. *et al.* C5L2, a nonsignaling C5A binding protein. *Biochemistry* **42**, 9406–9415 (2003).
37. Pandey, S. *et al.* Intrinsic bias at non-canonical, β-arrestin-coupled seven transmembrane receptors. *bioRxiv* 2021.02.02.429298 (2021) doi:10.1101/2021.02.02.429298.
38. Kumari, P. Novel insights into GPCR- β -arrestin interaction and signaling. (2019).
39. Shukla, A. K. *et al.* Visualization of arrestin recruitment by a G-protein-coupled receptor. *Nature* **512**, 218–222 (2014).
40. Oakley, R. H., Laporte, S. A., Holt, J. A., Caron, M. G. & Barak, L. S. Differential Affinities of Visual Arrestin, βArrestin1, and βArrestin2 for G Protein-coupled Receptors Delineate Two Major Classes of Receptors*. *J. Biol. Chem.* **275**, 17201–17210 (2000).
41. Baidya, M. *et al.* Genetically encoded intrabody sensors report the interaction and trafficking of b -arrestin 1 upon activation of G-protein – coupled receptors. **295**, 10153–10167 (2020).
42. Croker, D. E. *et al.* Discovery of functionally selective C5aR2 ligands: novel modulators of C5a signalling. *Immunol. Cell Biol.* **94**, 787–795 (2016).
43. Croker, D. E. *et al.* C5a2 can modulate ERK1/2 signaling in macrophages via heteromer formation with C5a1 and β-arrestin recruitment. *Immunol. Cell Biol.* **92**, 631–639 (2014).
44. Dwivedi, H., Baidya, M. & Shukla, A. K. GPCR Signaling: The Interplay of Gαi and β-arrestin. *Curr. Biol.* **28**, R324–R327 (2018).
45. Grundmann, M. *et al.* Lack of beta-arrestin signaling in the absence of active G proteins. *Nat. Commun.* **9**, 341 (2018).
46. Wang, J. *et al.* Gα(i) is required for carvedilol-induced β(1) adrenergic receptor β-arrestin biased signaling. *Nat. Commun.* **8**, 1706 (2017).
47. Cahill, T. J. *et al.* Distinct conformations of GPCR–β-arrestin complexes mediate desensitization, signaling, and endocytosis. *Proc. Natl. Acad. Sci.* **114**, 2562 LP – 2567 (2017).
48. Kumari, P. *et al.* Functional competence of a partially engaged GPCR–β-arrestin complex. *Nat. Commun.* **7**, 13416 (2016).
49. Kumari, P. *et al.* Core engagement with β-arrestin is dispensable for agonist-induced vasopressin receptor endocytosis and ERK activation. *Mol. Biol. Cell* **28**, 1003–1010 (2017).

50. Staus, D. P. *et al.* Structure of the M2 muscarinic receptor–β-arrestin complex in a lipid nanodisc. *Nature* **579**, 297–302 (2020).
51. Lee, Y. *et al.* Molecular basis of β-arrestin coupling to. (2020) doi:10.1038/s41586-020-2419-1.
52. Huang, W. *et al.* Structure of the neurotensin receptor 1 in complex with β-arrestin 1. *Nature* (2020) doi:10.1038/s41586-020-1953-1.
53. Yin, W. *et al.* A complex structure of arrestin-2 bound to a G protein-coupled receptor. *Cell Res.* **29**, 971–983 (2019).
54. Chaturvedi, M., Maharana, J. & Shukla, A. K. Terminating G-Protein Coupling: Structural Snapshots of GPCR-β-Arrestin Complexes. *Cell* **180**, 1041–1043 (2020).

I, Shubhi Pandey, hereby declare that the information contained herein is true and correct to the best of my knowledge and belief.

Shubhi Pandey